Sedimentary Geology 461 (2024) 106575

Contents lists available at ScienceDirect

Sedimentary Geology

journal homepage: www.elsevier.com/locate/sedgeo

Carbonate factory response through the MECO (Middle Eocene Climate Optimum) event: Insight from the Apulia Carbonate Platform, Gargano Promontory, Italy

C. Morabito [a], C.A. Papazzoni [b], D.J. Lehrmann [c], J.L. Payne [d], K. Al-Ramadan [e], M. Morsilli [a,*]

[a] Dipartimento di Fisica e Scienze della Terra, Università di Ferrara, 44122 Ferrara, Italy
[b] Dipartimento di Scienze Chimiche e Geologiche, Università di Modena e Reggio Emilia, 41125 Modena, Italy
[c] Department of Geosciences, Trinity University, San Antonio, TX 78212, USA
[d] Department of Geological Sciences, Stanford University, Stanford, CA 94305, USA
[e] College of Petroleum Engineering & Geosciences, King Fahd University of Petroleum & Minerals, 31261 Dhahran, Saudi Arabia

ARTICLE INFO

Article history:
Received 22 November 2023
Received in revised form 21 December 2023
Accepted 22 December 2023
Available online 5 January 2024

Dataset link: Isotopic dataset Monte Saraceno (Original data)

Editor: Dr. Catherine Chagué

Keywords:
Carbonate factories
MECO
Apulia
Middle Eocene
Large Benthic Foraminifera
Corals

ABSTRACT

During the Eocene, shallow-water carbonate systems were significantly impacted by climate fluctuations and hyperthermal events. Following the peak temperatures of the Early Eocene Climatic Optimum (EECO), a general cooling trend began, with short-lived (~200 kyr) warming events occurring alongside it. In the early Bartonian (around 40.1 Ma), a warming event known as the Middle Eocene Climatic Optimum (MECO) occurred, lasting approximately 500,000 years. In this scenario, the types and calcification rates of marine organisms such as corals and larger benthic foraminifera (LBF) were influenced by global CO_2 and oceanographic changes, which had a major effect on photic carbonate factories. To better understand the effects of these factors on carbonate factories, a detailed study of shallow-water facies types, distributions, and evolution was conducted. The Middle Eocene Monte Saraceno sequence, located on the eastern margin of the Apulia Carbonate Platform (Gargano Promontory, southern Italy), was selected as a case study to investigate the relationships between carbonate factory types and climatic changes around the MECO event. This study identified two distinct intervals with different modes of carbonate production, separated by a sharp boundary. The lower interval consists of clinostratified, thick beds of rudstone to floatstone, mostly made up of various large *Nummulites* tests, indicating an early Bartonian age (Shallow Benthic Zone 17). Instead, the upper interval consists of coral floatstone to rudstone with a packstone matrix, rich in branching corals in association with gastropods, bivalves, and rare small larger benthic foraminifera. The appearance of *Heterostegina* sp. and *Glomalveolina ungaroi* in this interval indicates a late Bartonian age (Shallow Benthic Zone 18). By integrating biostratigraphic and stable-isotope data, the lower interval, with abundant *Nummulites*, was linked to the MECO event, during which higher sea-surface temperatures seem to enhance larger benthic foraminifera proliferation, as already occurred in the Early Eocene. However, in the late Bartonian, the sharp transition to a coral-dominated carbonate factory, with rare larger benthic foraminifera showing smaller sizes, could be attributed to a drop in temperature that created the conditions more favourable to corals. Overall, this study provides compelling evidence of how environmental changes can affect marine carbonate production, also highlighting the importance of investigating these relationships, to better understand climate change in the past, present and near future.

1. Introduction

Significant transient and long-term changes occurred in Earth's climate during the Paleaogene, culminating in the transition from global greenhouse to icehouse conditions (Zachos et al., 2001). Due to its general warmth and high atmospheric pCO_2, the Eocene Epoch (56 to 34 million years ago) may be used as a reference model for predicting future climate conditions. The Paleaocene–Eocene boundary was marked by a pronounced but transient warming event (Paleaocene–Eocene Thermal Maximum: PETM), followed by increasingly high temperatures culminating in the Early Eocene Climatic Optimum (EECO) in the late Ypresian; to this extreme warming followed a gradual cooling trend lasted up to the Eocene–Oligocene transition. In the early Eocene, high levels of atmospheric CO_2 led to extremely warm climate and decreased meridional temperature gradients (Van

* Corresponding author.
E-mail address: mrh@unife.it (M. Morsilli).

https://doi.org/10.1016/j.sedgeo.2023.106575

der Ploeg et al., 2023). Subsequently, during the Middle Eocene, the general cooling trend was episodically interrupted by transient climate warming events, most of them short-lived (<200 kyr). During the early Bartonian (at ~40.1 Ma), a ~500 kyr warming event occurred, known as the Middle Eocene Climatic Optimum (MECO). This interval has been identified in the Southern, Atlantic, Pacific, Indian and Tethyan Oceans (Bohaty and Zachos, 2003; Jovane et al., 2007; Bohaty et al., 2009; Cramwinckel et al., 2018; Giorgioni et al., 2019). It was associated with pronounced changes in the hydrosphere, atmosphere, and biosphere. The $\delta^{18}O$ records indicate a global warming of ca. 4 to 6 °C of both surface and deep waters, which was associated with shoaling of the calcite compensation depth (Bohaty et al., 2009; Edgar et al., 2010) and elevated pCO_2 (Bijl et al., 2010).

Important evidence of the MECO comes from sediment cores in the Indian and Atlantic sectors of the Southern Ocean. Here, a negative shift in $\delta^{18}O$ values at 41.5 Ma, followed by a 1.8 ‰ increase in benthic $\delta^{18}O$ values between ca. 41 and 37 Ma, interpreted as ~6 °C cooling, has been recognized (Bohaty and Zachos, 2003; Edgar et al., 2010). Bohaty et al. (2009), Edgar et al. (2010), and Khanolkar et al. (2017), among others, show a negative CIE during the MECO event. Conversely, in Italy, this hyperthermal event has been identified in two deep-water sections, the Contessa and Alano sections. Here, high-resolution palaeomagnetic investigation and analyses of planktonic and benthic foraminifera integrated with oxygen and carbon isotope measurements have been conducted (Jovane et al., 2007; Boscolo Galazzo et al., 2013; Luciani et al., 2010; Spofforth et al., 2010). According to Jovane et al. (2007) and Boscolo Galazzo et al. (2013), the $\delta^{13}C$ curve of Contessa and Alano sections presents a positive peak, which for the Contessa section corresponds to 0.6 ‰ at 40 Ma. It represents the first evidence in the northern hemisphere of the MECO, comparable with the stable isotope anomaly observed in the Indian–Atlantic sector by Bohaty and Zachos (2003).

Moreover, the evolution of shallow-water carbonate factories is subject to the influence and control of various factors, such as global and regional fluctuations in climate, global and local tectonic activity, changes in eustatic sea levels, and the evolution of benthic biota over time (Höntzsch et al., 2013). Throughout the Eocene, the high temperatures favoured the calcitic larger benthic foraminifera (LBF) flourishing in the shallow-marine carbonate environments of the Tethys (Pomar et al., 2017). LBF, as important carbonate producers, represent powerful bioindicators (proxies) of environmental changes (Wilson, 2008; Pomar et al., 2012).

Specifically, the EECO (52–49 Ma; Zachos et al., 2001) and the post-PETM events coincide with peaks in the species-level diversity of K-strategist LBF (Hottinger, 1998; Höntzsch et al., 2011). Likewise, from the middle Ypresian up to the Bartonian, the size of LBF increased significantly (Hottinger, 2001). In addition, the early to late Bartonian boundary has been recognized as crucial time for the biological change in the Tethys realm (Martín-Martín et al., 2021). During this period, biota such as LBF and scleractinian corals were strongly affected by these changes. Variations in benthic foraminiferal assemblages mainly indicate changes in water depth, organic matter flux to the seafloor, oxygenation and temperature (e.g., Gooday, 2003; Murray, 2006). During the Middle Eocene, the dominant biota were large nummulitids belonging to the genera *Nummulites* and *Assilina*. Additionally, alveolinids were quite abundant during this time, even if their maximum diversification dates back to the Early Eocene. Right before the Late Eocene, the nummulite lineages with reticulate surfaces started their evolution, accompanied by small radiate forms and new genera with chambers subdivided into chamberlets, such as *Heterostegina* and *Spiroclypeus*. Moving into the early Oligocene, the LBF fauna became less diversified, with the extinction of the orthophragmines and a few species of the genus *Nummulites*.

LBF required similar ecological conditions, e.g. nutrients, light, tropical and subtropical water temperature of other organisms as z-corals (Hottinger, 1983; Hallock, 1985, 2000) occupying similar ecological niches (Martín-Martín et al., 2021). However, their response to the temperature increasing, UV exposure and/or presence of nutrients, seems to be different. Specifically, when the temperature exceeds the corals' threshold, they expel their symbiont algae, leading to bleaching (Hallock, 2000; Höntzsch et al., 2013; Pomar et al., 2017). Hence, important producers of $CaCO_3$, such as corals and larger benthic foraminifera (Langer, 2008), were sensitive to changes in water quality. Examples of LBF–coral co-existence have been described from the late Palaeocene up to Lutetian Sierra Espuña–Mula Basin successions (Betic Cordillera, S Spain), the Moroccan Ghomarides Domain (Moroccan Internal Rif Zone) (Martín-Martín et al., 2020, 2021, 2023; Tosquella et al., 2022), and the Priabonian Nago Limestone (northern Italy) (Luciani, 1989; Bassi, 1998; Bosellini and Papazzoni, 2003). However, the Eocene was considered a transitional period for the coral reef evolution in which the warm hyperthermal events, including MECO, seem to be detrimental for the coral's growth (Martín-Martín et al., 2021; El-Azabi, 2023). This carbonate factory variation is likewise observed in various locations, including the Mossano section (Italy), the Prebetic platform and Betic Cordillera (southern Spain), the Maiella platform (Italy), the Gavrovo–Tripolitza area (Greece), northern and central Turkey, Tunisia, and the El-Ramliya area (Egypt). In Greece and the Maiella platform, coral reefs became significant contributors to the platform during the Priabonian, although they were generally present but not as prominent during the early–middle Eocene (Moussavian and Vecsei, 1995; Vecsei and Moussavian, 1997; Barattolo et al., 2007). In NW Turkey, the Thrace Basin during the Early Eocene was dominated by larger benthic foraminifera, with the first coral reefs appearing in the upper Bartonian and becoming more prominent in the late Bartonian to Priabonian (Middle–Late Eocene) (Özcan et al., 2010; Less et al., 2011). Studies on the Prebetic platform (SE Spain) indicate a dominance of LBF and coralline red algae during the Eocene, with a gradual decrease in orthophragminids and nummulitids towards the upper part of the Middle Eocene succession. The occurrence of corals was associated with the global cooling event at the Bartonian–Priabonian boundary (Höntzsch et al., 2013). These biological changes were also observed by Martín-Martín et al. (2021) in the Sierra Espuña–Mula basin in the Betic Cordillera, southern Spain, in which the early–late Bartonian boundary (SBZs 17–18) was characterized by biological change, including the end of increasing LBF test sizes linked to increased heterotrophism in shallow-marine waters and a recovery of zooxanthellate corals. In the Siouf Member of Tunisia, the abundance of *Nummulites* is linked to the Middle Eocene Climatic Optimum (MECO) warming peak also correlated with a rapid sea level rise and the development of a shallow-water carbonate platform in central Tunisia from 40.5 Ma to 39.8 Ma (Messaoud et al., 2023). Likewise, in the El-Ramliya area (Egypt), El-Azabi (2023) linked the corals (*Acropora* genus) lacking during the Bartonian age, to the warm temperatures reached during the MECO event.

The detailed study of the palaeoenvironments and related facies evolution of the Middle Eocene Monte Saraceno sequence, promises to be a useful case study to identify short and long-term environmental changes in the shallow-water domain. In particular, the main purpose of this work is: i) to interpret the carbonate facies shift between the lower nummulitic and upper corals facies; ii) to investigate the impact of the MECO event on a shallow water succession, also exploring the evolution of a carbonate ramp system across this time; and iii) to increase the "knowledge of the geological record" of LBF–coral response to the MECO event.

2. Geological and stratigraphic setting

The Gargano Promontory (Fig. 1A), located in the Apulia Region (Southern Italy), is the foreland of the Southern Apennine orogenic system. This area was slightly deformed and uplifted during the Neogene period, primarily as the result of the tectonic activity associated with the Apennine and Dinaric thrust belt convergence (Doglioni et al., 1994; Bertotti et al., 1999; Brankman and Aydin, 2004).

The Gargano Promontory belongs to the Apulian Carbonate Platform (ACP, Fig. 1B) and was a major palaeogeographic element of the southern

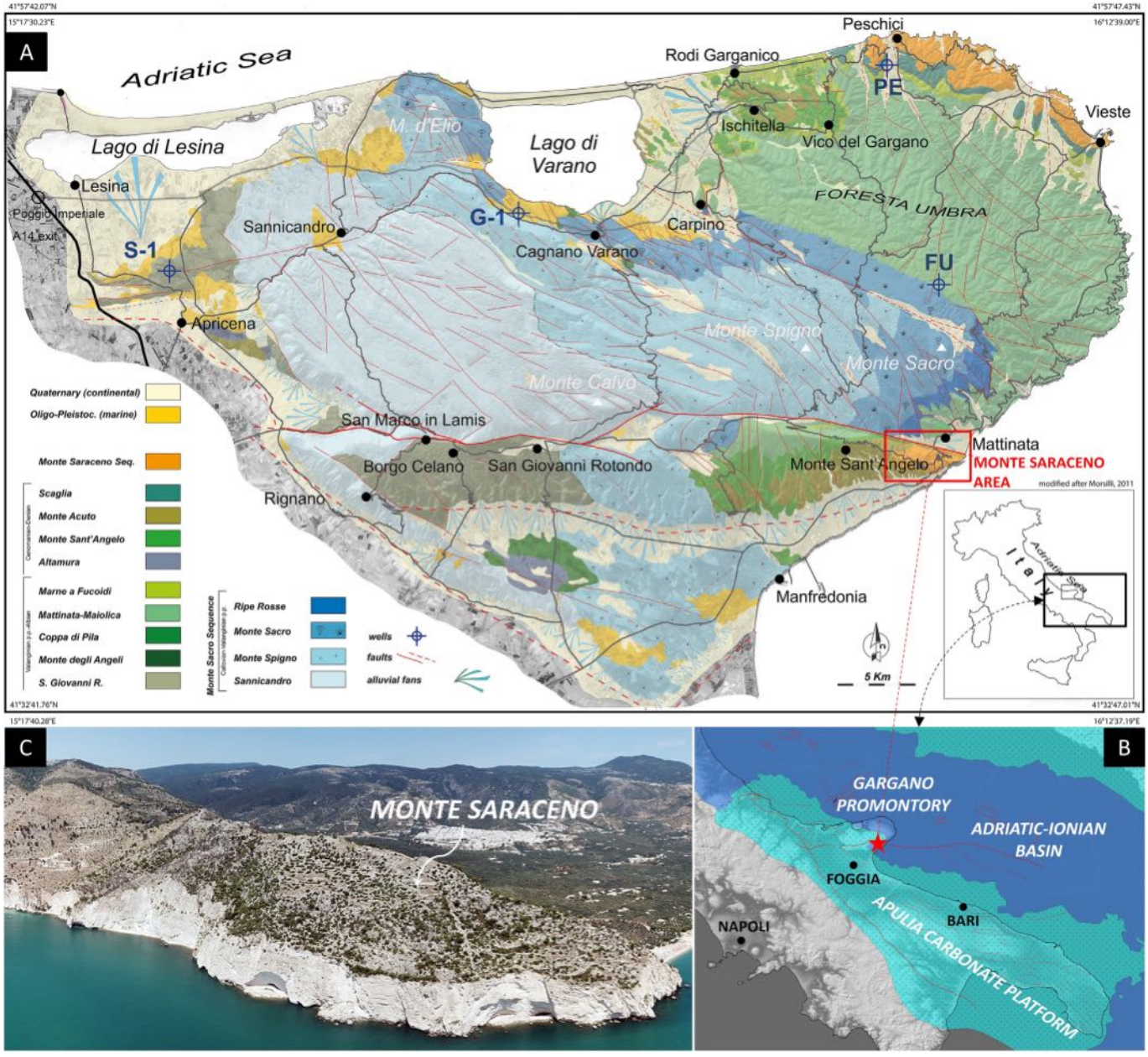

Fig. 1. A) Geological map of the Gargano Promontory (modified after Morsilli et al., 2017); B) Apulian Carbonate Platform reconstruction based on offshore seismic profiles and exploration wells (based on Morsilli et al., 2017); C) aerial photograph of the investigated area (Monte Saraceno).

passive margin of the Tethys Ocean formed during Jurassic and Cretaceous time. The ACP is one of the so-called peri-Adriatic platforms partially comparable to the Bahama banks in terms of facies, shape, size and also in the internal architecture (Eberli et al., 1993; Bosellini et al., 1999; Morsilli et al., 2017, 2021).

The Gargano Promontory consists of a thick succession of Jurassic to Eocene carbonate rocks (Fig. 1A) with different facies belts including inner platform, margin and slope-to-basin deposits (Morsilli and Bosellini, 1997; Bosellini et al., 1999; Borgomano, 2000; Morsilli et al., 2004, 2017; among others). The various stratigraphic units have been organized into depositional supersequences on the basis of the occurrence of various types of unconformities (Bosellini et al., 1999; Morsilli et al., 2021), such as the Eocene Monte Saraceno Sequence, which is characterized by an extensive basal disconformity. In the Monte Saraceno area (Fig. 1C), this 250 m-thick sequence starts with a megabreccia interval (Grottone Megabreccia — late Ypresian?), followed by Lutetian–Bartonian calcarenitic deposits (Coppa d'Apolito Calcarenite and Monte Saraceno Limestone), passing to coeval pelagic deposits of the Scaglia Formation known locally as the Punta Rossa Limestone (Bosellini and Neri, 1995; Bosellini et al., 1999; Adams et al., 2002; Matteucci et al., 2012; Morsilli et al., 2021). Instead, in the north-eastern part of the Gargano, a 350 m-thick interval of middle Eocene calciturbidites and scattered breccia beds (Peschici Formation; Bosellini et al., 1993) covers disconformably the Upper Cretaceous basinal deposits of the Scaglia Formation, above an important hiatus (Fig. 1A).

In detail, the formations belonging to the Monte Saraceno Sequence (Fig. 2) are:

i. *Grottone Megabreccia*. This unit, 50–60 m thick, consists mainly of thick breccia and megabreccia beds, frequently amalgamated, made of several channelized bodies. It has been interpreted to have formed

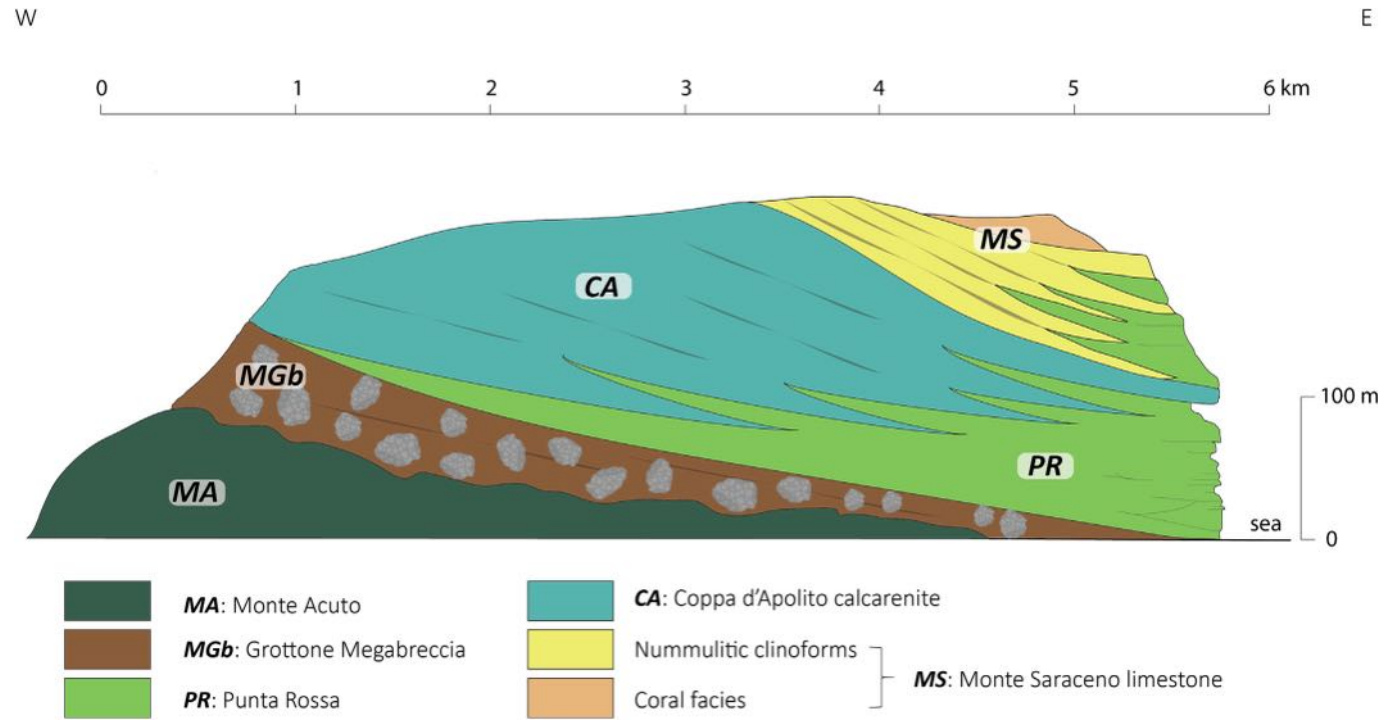

Fig. 2. Stratigraphic relationships among the units of the Monte Saraceno sequence. (Modified after Bosellini and Neri (1995).)

via repeated catastrophic margin collapses with rock falls and debris-flow episodes that caused partial dismantling of the Cretaceous–Palaeocene and early Eocene deposits (Bosellini et al., 1999).

ii. *Punta Rossa Limestone*. This is the middle Eocene basinal (proximal) facies, consisting of chalky, whitish and sub-horizontal, thin-bedded lime mudstone. This unit crops out spectacularly along the 50–60 m-high white sea-cliff of the Monte Saraceno (see Fig. 1B). There are several 20–30 cm thick calciturbidites within the succession, which appear to be characterized by frequent truncation surfaces and discordances (slump scars).

iii. *Coppa d'Apolito Calcarenite*. This unit mostly consists of fine-grained calcarenites, which are frequently bioturbated and amalgamated, and thin to medium calciturbidite beds, sometimes channelized, full of LBF (*Discocyclina* and *Nummulites*). Rare breccia layers, with clasts and matrix derived from the same unit, occur locally. Cemented patches or cemented layers, attributed to concretionary calcite cementation, are the striking feature of this unit.

iv. *Monte Saraceno Limestone*. This is the uppermost unit of the sequence and is represented by clinostratified, coarse calcarenites and rudstones, consisting mostly of nummulitids capped by a floatstone with abundant branching corals and subordinated gastropods and bivalves. The nummulitic clinoforms, with a variable inclination from 16° to 25°, pass laterally to basinal stratified deposits of Punta Rossa Limestone (Adams et al., 2002). This unit was interpreted by Bosellini et al. (1999) as a proximal slope passing to small patch-reefs growing on the deeper margin and probably related to a sea-level drop (lowstand shelf edge — forced regression). Adams et al. (2002) provide a detailed facies description of the Monte Saraceno carbonate system, focusing attention on the relationship between slope inclination and sediment fabric. He describes four different slope facies in detail: facies 1) packstone–grainstone with larger foraminifera (*Nummulites*, *Discocyclina*), benthic smaller foraminifera (rotaliids, miliolids, textulariids), echinoid spines and shell fragments; facies 2) skeletal packstone to rudstone with larger foraminifera (*Nummulites*, *Discocyclina*), benthic smaller foraminifera (rotaliids, miliolids), echinoid spines and fragmented shells; 3) packstone with larger foraminifera (*Gypsina*, *Alveolina*, *Asterigerina*), benthic smaller foraminifera (rotaliids, textulariids), red and green algae, echinoid fragments and bivalve shell fragments; 4) packstone to floatstone with in situ corals and coral fragments, larger foraminifera (*Nummulites*, *Gypsina*, *Asterigerina*), benthic smaller foraminifera (textulariids), coralline algae and echinoid spines.

v. *Peschici Formation*. This is a thick succession (350 m) of graded breccias and calciturbidites alternating with thin pelagic lime-mudstone. This unit crops out outside of our study area (see Fig. 1A). The basal contact is a spectacular marine onlap that infills a huge submarine scar, deeply eroded into underlying Upper Cretaceous Scaglia Fm (Bosellini et al., 1999; Morsilli et al., 2021). The large hiatus between the Peschici Fm and Scaglia Fm has also been recognized in the Adriatic offshore in some exploration wells (De Alteriis and Aiello, 1993).

Previous authors determined the age of the Monte Saraceno deposits based on the larger foraminiferal assemblages, especially with reference to the genus *Nummulites*. Tellini (1890) in a complete revision of the nummulites of the Gargano Promontory, Tremiti and Maiella area, was the first author to recognize and collect the *Nummulites* species around the Monte Saraceno area. Later Matteucci (1971, 1978) and Matteucci et al. (2012), based on the foraminiferal assemblages, assigned the Monte Saraceno nummulitic zone to the upper Lutetian (SBZs 15–16) and lower Bartonian (SBZ 17), sensu Serra-Kiel et al. (1998). He assigned to the early Bartonian (SBZ 17) the Monte Saraceno Limestone, due to the occurrence of *Nummulites brongniarti* (SBZ 17) (Matteucci et al., 2012).

In this study, on the basis of the identified skeletal components, we assign to the SBZ 17 (lower Bartonian) the Monte Saraceno clinoforms; the occurrence of *Heterostegina* sp. and *Glomalveolina ungaroi* in the uppermost coral facies, indicates a middle to upper Bartonian (SBZ 18, sensu Less et al., 2008).

3. Material and methods

In order to reach the goals of this study, the standard methodology based on the field observations, sampling, measurement of stratigraphic logs, detailed facies mapping and laboratory analysis has been applied.

The sedimentary lithofacies were characterized through the outcrop observation whilst, the laboratory study, was subdivided into microscope observation and stable isotope analysis ($\delta^{13}C$, $\delta^{18}O$), performed at the Laboratory of Paleoclimatology and Isotope Stratigraphy (Ferrara, Italy).

176 samples and 110 thin sections have been studied under an optical microscope for the microfacies and fossil assemblage characterization. In particular, grain types and size, texture, diagenetic features, and the skeletal grains and biostratigraphic distribution of the LFB have been reported. Dunham (1962) and Insalaco (1998) classifications were used to classify the textures. Depositional textures for lithofacies definition were analysed semi-quantitatively and expressed in terms of relative abundance.

For geochemical analysis, the lime mudstone part of 134 samples has been microdrilled and analysed for $\delta^{13}C$ and $\delta^{18}O$ values. To avoid large bioclasts or recrystallization, the polished slabs were studied under a binocular microscope and checked with the respective thin sections before the microdilling. All results are reported in per mil (‰), in the conventional δ notation with reference to the Vienna Pee Dee Belemnite (VPDB) standard.

4. Results

4.1. Monte Saraceno section

To thoroughly analyse the depositional geometries, architecture, and spatial distribution, a comprehensive lithofacies map was created at a scale of 1:5000. This detailed map allows for a close examination of the various lithofacies present in the study area, providing insights into their characteristics, lateral extension and stratigraphic relationships, and distribution patterns. The map represents a valuable tool in understanding depositional geometries, facies transitions, sedimentary environments, and the overall geological context (Fig. 3).

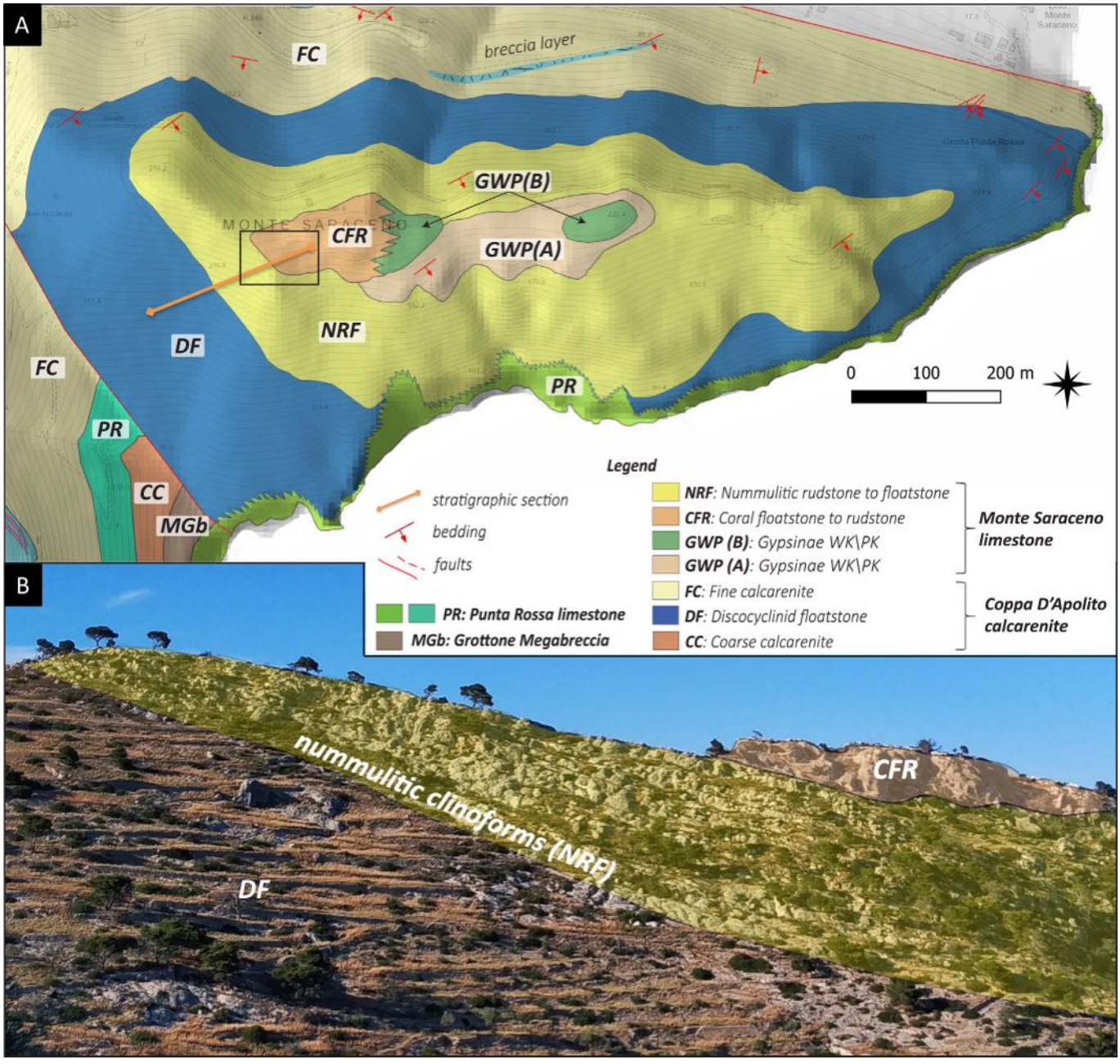

Fig. 3. A) Lithofacies map of the Monte Saraceno area with location of the stratigraphic section (orange line). The black box identifies the detailed log along the section. B) Panoramic view showing the carbonate facies shift between the lower nummulitic clinoforms (NRF) and the upper coral facies (CFR).

The stratigraphic section, measured from the upper interval of the Coppa d'Apolito Calcarenite to the top of Monte Saraceno Limestone (41° 41′ 38.04″ N; 16° 03′ 9.88″ E) with a total thickness of 104.5 m, highlights the different lithofacies associations (Fig. 4). Moreover, the upper 31.5 m of the studied section, where a transition in carbonate factories occurs between the nummulite-rich

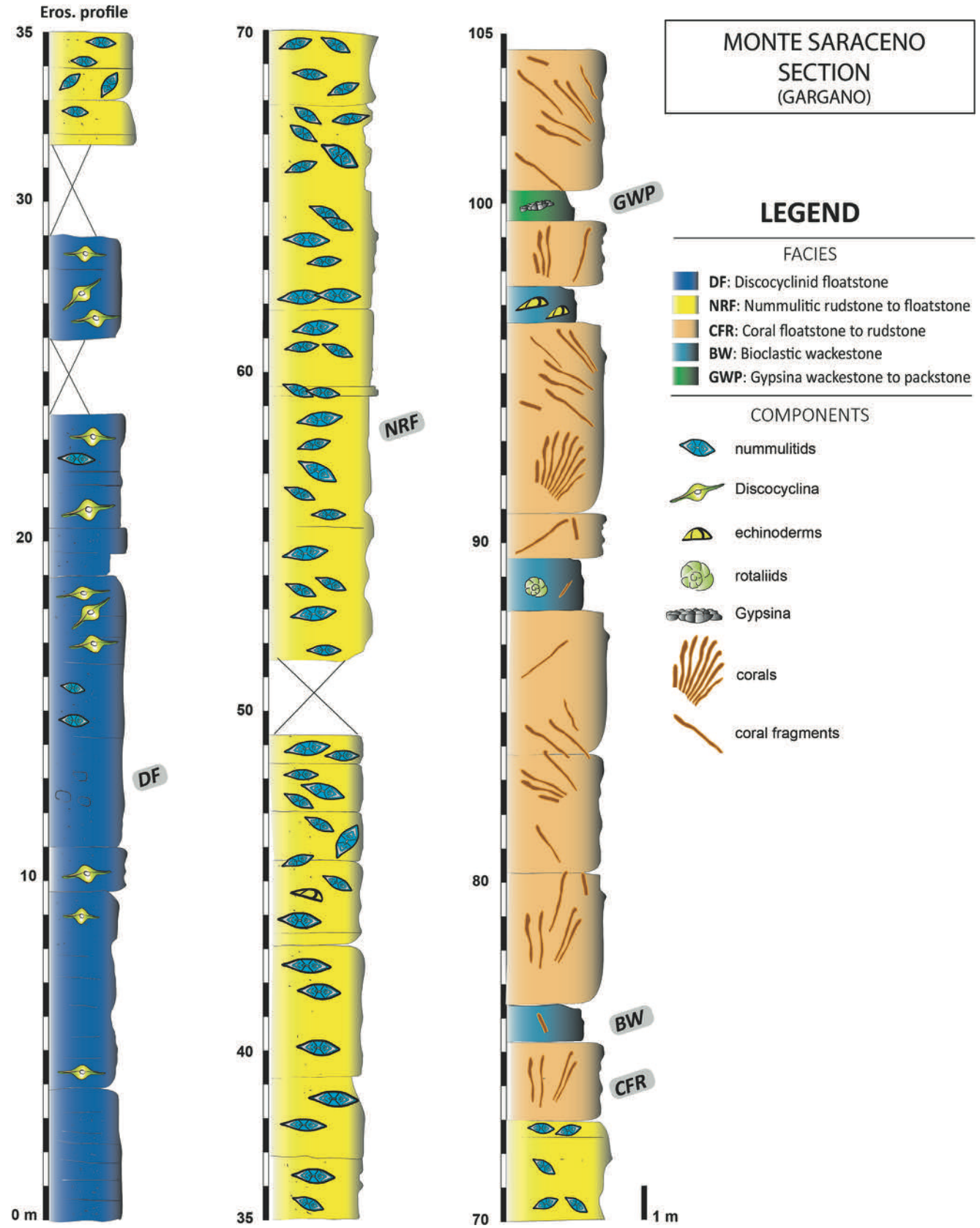

Fig. 4. Stratigraphic section of Monte Saraceno. The NRF, CFR, BW, and GWP lithofacies belong to Monte Saraceno Limestone and DF lithofacies to the upper interval of Coppa D'Apolito Calcarenite.

clinoforms and coral facies, is exceptionally well exposed and has undergone detailed analysis.

4.2. Lithofacies

Based on analysis of textures and skeletal components both in outcrop and thin sections, five main lithofacies have been distinguished (Fig. 5; Table 1): i) Discocyclinid floatstone (DF); ii) nummulitic rudstone to floatstone (NRF); iii) coral floatstone to rudstone (CFR); iv) *Gypsina* wackestone to packstone (GWP); and v) bioclastic wackestone (BW).

4.2.1. DF — discocyclinid floatstone

This floatstone very rich in LBF, with a packstone to grainstone matrix, contains a great abundance of orthophragmins associated with nummulitids. The LBF association, characterized by *Discocyclina* and *Nummulites* presents also small rotaliids (some *Asterigerina rotula*),

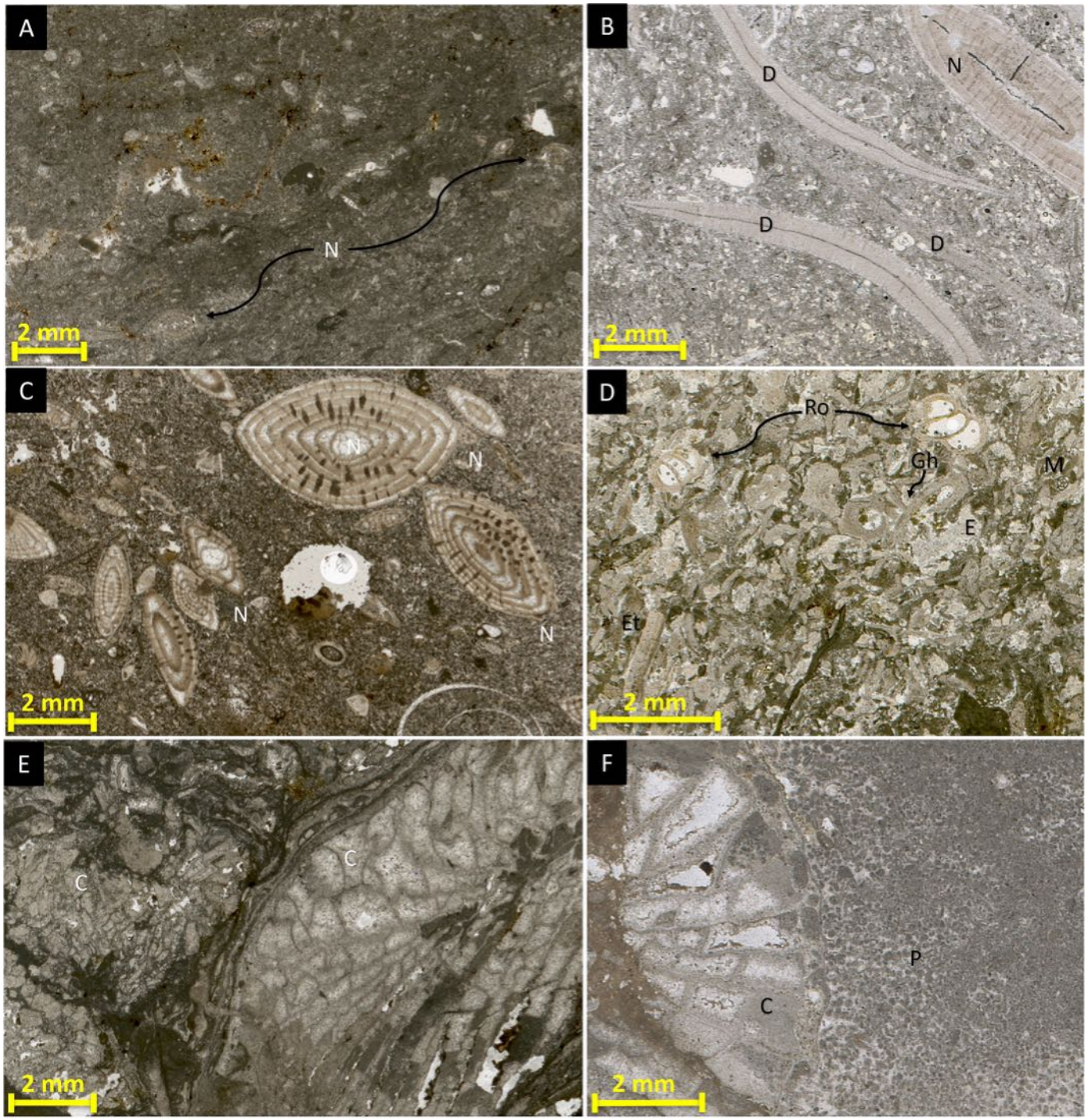

Fig. 5. Photomicrographs of the identified lithofacies (plane polarized light). (A–B) *Nummulites* size variation in nummulitic rudstone to floatstone facies. A) Packstone to wackestone dominated by small nummulites (about 2 mm in diameter); B) floatstone with discocyclinids and *Nummulites* (DF); C) MS(A) 1.2 sample characterized by large nummulites (about 6 mm in diameter); D) *Gypsina* wackestone to packstone (GWP); E–F) floatstone to rudstone with coral fragments and peloid facies CRF; P = peloids; C = corals; Gh = *Gypsina* hook-shaped; E = echinoderms; Ro = rotaliids; Et = *Ethelia alba*; N = *Nummulites*; D = *Discocyclina*.

Table 1
Recognized lithofacies of Monte Saraceno section with the relative abundance of components. Studied samples and fossil content (common, abundant, present and/rare) are also shown.

Lithofacies		Fossils and non-skeletal grains common and/or abundant*	Fossils and non-skeletal grains present and/or rare
DF	Discocyclinid floatstone	*Nummulites**, *Discocyclina**, bivalves, echinoderms, miliolids	Textulariids, small rotaliids, Corallinaceean red algae, acervulinids
NRF	Nummulitic rudstone to floatstone	*Nummulites**, *Asterigerina rotula*, peloids	*Gypsina* hook-shaped, *Gypsina*, miliolids, *Gyroidinella magna*, discorbids, textulariids, articulated red algae (fragments), echinoderms
CFR	Coral floatstone to rudstone	Corals*, peloids*, *Gypsina*, miliolids, echinoderms	Small thick *Nummulites*, *Gypsina* hook-shaped, *Sphaerogypsina globula*, *Asterigerina rotula*, *Gyroidinella magna*, *Heterostegina*, discorbids, textulariids, small rotaliids, articulated red algae, non-articulated red algae (*Sporolithon*), Corallinaceean algae (*Lithoporella*), bryozoans, gastropods
BW	Bioclastic wackestone	Echinoderms	Bivalve shells, *Asterigerina rotula*, *Heterostegina*, *Operculina*, coral fragments, peloids
GWP(A)	*Gypsina* wackestone to packstone with *Nummulites*	*Gypsina**, *Gypsina* hook-shaped, peloids, discorbids, echinoderms, articulated red algae	Small thick *Nummulites*, *Operculina*, *Gypsina linearis*, *Sphaerogypsina globula*, miliolids, *Planorbulina*, *Asterigerina rotula*, *Gyroidinella magna*, *Fabiania cassis*, *Mississippina binkhorsti*, textulariids, unspecific rotaliids, bivalve shells, *Ethelia alba*?, *Lithoporella*, bryozoans
GWP(B)	*Gypsina* wackestone to packstone with corals	*Gypsina**, *Gypsina* hook-shaped, miliolids, *Gyroidinella magna*	Coral fragments, textulariid, small rotaliids, *Heterostegina*, *Glomalveolina ungaroi*, *Gypsina linearis*, *Fabiania cassis*, *Pyrgo*, echinoderms

miliolids, textulariids and acervulinids. Furthermore, coralline red algal fragments, bivalve shells and echinoid plates are common.

4.2.2. NRF — nummulitic rudstone to floatstone

This lithofacies is characterized by clinostratified thick rudstone to floatstone beds with abundant LBF. They are represented by the large nummulitids (*Nummulites*) mostly at the bottom of the section becoming smaller going up through the section (Fig. 5A). Furthermore, some rotaliids (*Asterigerina rotula* often dissolved, *Rotaliconus*), textulariids, Miliolids, *Gypsina* (rarely hook-shaped), molluscs (bivalves and rare gastropods), echinoids, ostracods, red algal fragments (articulated and non-articulated), and scattered bryozoan are also present.

4.2.3. CFR — coral floatstone to rudstone

This lithofacies, that corresponds to the uppermost part of the Monte Saraceno log (see Fig. 4), is characterized by yellowish rudstone to floatstone in massive or amalgamated beds full of coral branches and branching colonies usually slightly reworked. In situ corals rarely occur, mostly in the lower part of this unit. The main components of the packstone matrix are peloids associated with coral fragments and red algae. Less abundant are echinoids, bivalves, ostracods, rotaliids (*Asterigerina rotula*, *Gyroidinella magna*), textulariids and rare planktonic foraminifera. Specifically, articulated, non-articulated red algal fragments (*Lithothamnion*) and Corallinaceean algae (*Lithoporella*) occur in the whole sections, whilst the association of green algae with miliolids, discorbids and acervulinids (*Gypsina*, *Sphaerogypsina*) is present only at the bottom of this stratigraphic unit, where *Heterostegina*, nummulits and encrusting foraminifera are rare.

4.2.4. BW — bioclastic wackestone

This lithofacies, laterally intercalated with coral floatstone to rudstone (CFR) lithofacies, is represented by skeletal components belonging to various taxa. There were recognized rotalids (rare *Asterigerina rotula*), *Heterostegina*, *Operculina*, textulariids, molluscs (bivalve shells), echinoids, ostracods, red algae and scattered coral fragments, sometimes dissolved.

4.2.5. GWP — Gypsina wackestone to packstone

This lithofacies is characterized by whitish to yellowish wackestone to packstone beds rich of acervulinids (*Gypsina linearis* and *Gypsina* frequently hook-shaped) with miliolids, small rotaliids, echinoids, bivalve shells, gastropods, bryozoans, Corallinaceean algae (*Lithoporella*), fragmented articulated red algae, and peloids. This facies occurred either in association with small *Nummulites* (*GWP(A)*), in the upper interval above the nummulitic clinoforms (see Fig. 3A), and inter-fingered, with the coral lithofacies (*GWP(B)*). Here the species *Glomalveolina ungaroi* and *Heterostegina* sp. occasionally occur within this facies.

4.3. LBF–coral facies shift

The upper part of the Monte Saraceno presents different skeletal components compared to the lower and the other parts of the investigated area.

At the uppermost level, a distinct surface marks the boundary between the clinostratified succession and a massive limestone enriched in fragments of branching corals, along with scattered in situ massive corals visible at a smaller scale (Fig. 6).

This important carbonate factory change has been described in the stratigraphic section, which focuses on the last 31.5 m of the entire measured section (Fig. 7).

Starting from the bottom, metric strata of rudstone to floatstone rich in nummulites associated with other smaller benthic foraminifera occur. The presence of large numbers of *Nummulites* of various sizes is the most prominent feature of this interval until a decrease, at about 3 m, either in size and abundance (see thin section pictures B–C of Fig. 6). The transitional zone is marked by a floatstone in a packstone–wackestone matrix in which small nummulitids (<2 mm), red algae, acervulinids, echinoid spines and sporadic miliolids are present. The entire nummulitic interval, from the base to the *Nummulites*–coral boundary, is totally lacking in coral fragments. The boundary between the nummulitic interval and the upper coral facies occurs at about 4 m. From here to the end of the section, 30 m of scattered branching coral's fragments, rarely including in-situ coral colonies, immersed in a peloidal wackestone to packstone matrix, laterally intercalated with the bioclastic wackestone (BW) and the *Gypsina* wackestone–packstone (GWP(B)) lithofacies appear.

4.4. Coral-rich interval

The upper part of the Monte Saraceno Limestone, characterized by the presence of numerous caves of variable size, with corals exposed in 3-dimensions within the caves, allows us to study from a macroscopic point of view the coral facies analysing their spatial distribution, morphology and internal structures with great detail. Here in-situ massive to platy coral colonies transitioning to chaotic breccias containing fragments of branching coral sticks occur. Within this interval, Matteucci et al. (2012) identified seventeen coral genera, including *Stylophora*, *Dendracis*, *Astreophora*, *Cyathoseris*, *Actinacis*, *Goniopora*, *Phyllocoenia*, *Cereiphillia*, *Antiguastraea*, *Leptomussa*, *Michelottiphyllia*, *Ilariosmilia*, *Plocophyllia*, and *Wellsia*. For the present study, two caves (A and B) have been examined (Fig. 8).

Cave A: Stratigraphically, the cave, 2 m high and 6 m wide, is set at a 12 metre height starting from large nummulite–coral facies transition. Specifically, the cave's walls point out numerous coral fragments with a branching structure and variable dimensions. Their

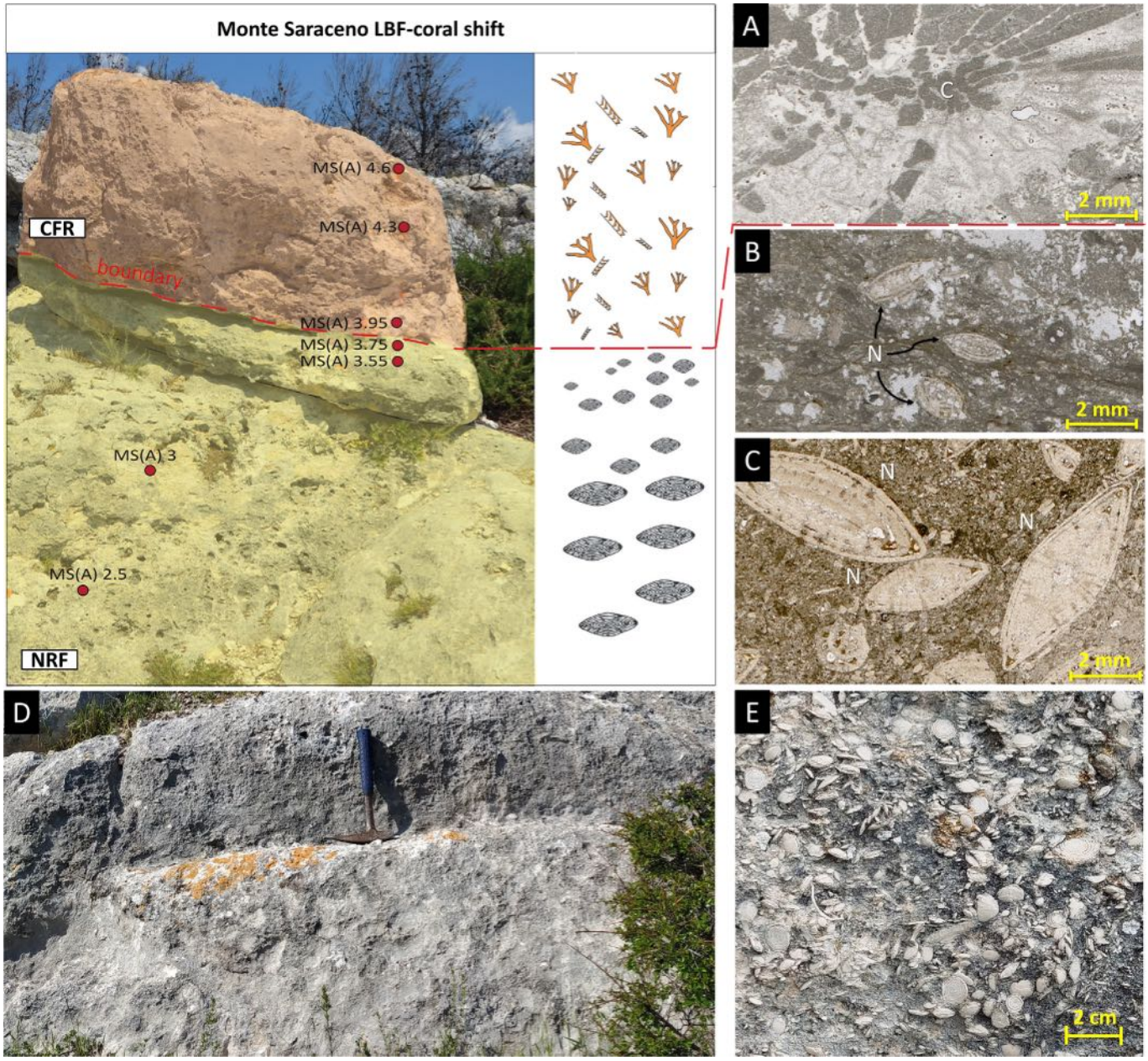

Fig. 6. Outcrop photos and thin section pictures highlighting the nummulite–coral facies shift. A) Coral floatstone to rudstone microfacies (CFR); B and C) nummulitic floatstone with small nummulites in the interval below the boundary (B), and the larger nummulites underlying (C); D and E) rudstone with nummulites in clinostratified layers. The red dots represent the location of the collected samples in this interval.

dimensions range from few centimetres up to 10–15 cm, immersed in a mudstone–wackestone matrix (Fig. 9).

Cave B: Cave B, located stratigraphically lower than the previous cave, with its 6 metre height and about 10 meter width, is the largest cave observed on the Monte Saraceno outcrop. Similar to the others, this cave is composed of coral fragments immersed in a fine-grained matrix. However, it represents the only cave in which it was recognized, in the lowest part, an isolated coral with platy morphology.

Summarizing, comparing both caves, most of the corals are branching or represented by fragments of branches. Furthermore, the spatial distribution of the fragments and the poor sorting suggest that transport is not related to a unidirectional flow but, rather, to a limited transport with a minimal coral reworking.

4.5. Stable isotopes

From the base to the top of the Monte Saraceno section, with a total thickness of 104,5 m, there is a gradual $\delta^{13}C$ decreasing trend starting from ~−0.62 ‰ to ~−4.67 ‰ values (Fig. 10A). However, the values between 21 and 31 m, corresponding to the upper part of the discocyclinid floatstone (DF) lithofacies, increase from −2.40 ‰ to −1.60 ‰ until reaching ~0.7 ‰ in $\delta^{13}C$ values in the upper 6 m, equivalent to the base of nummulitic rudstone to floatstone (NFR) facies. In addition, going upwards throughout the Monte Saraceno section, the curve highlights a gradual negative trend still related to the nummulitic abundance. This phase persists until the sharp negative CIE, linked to the carbonate facies shift to the coral facies and a reduction of the *Nummulites* genus

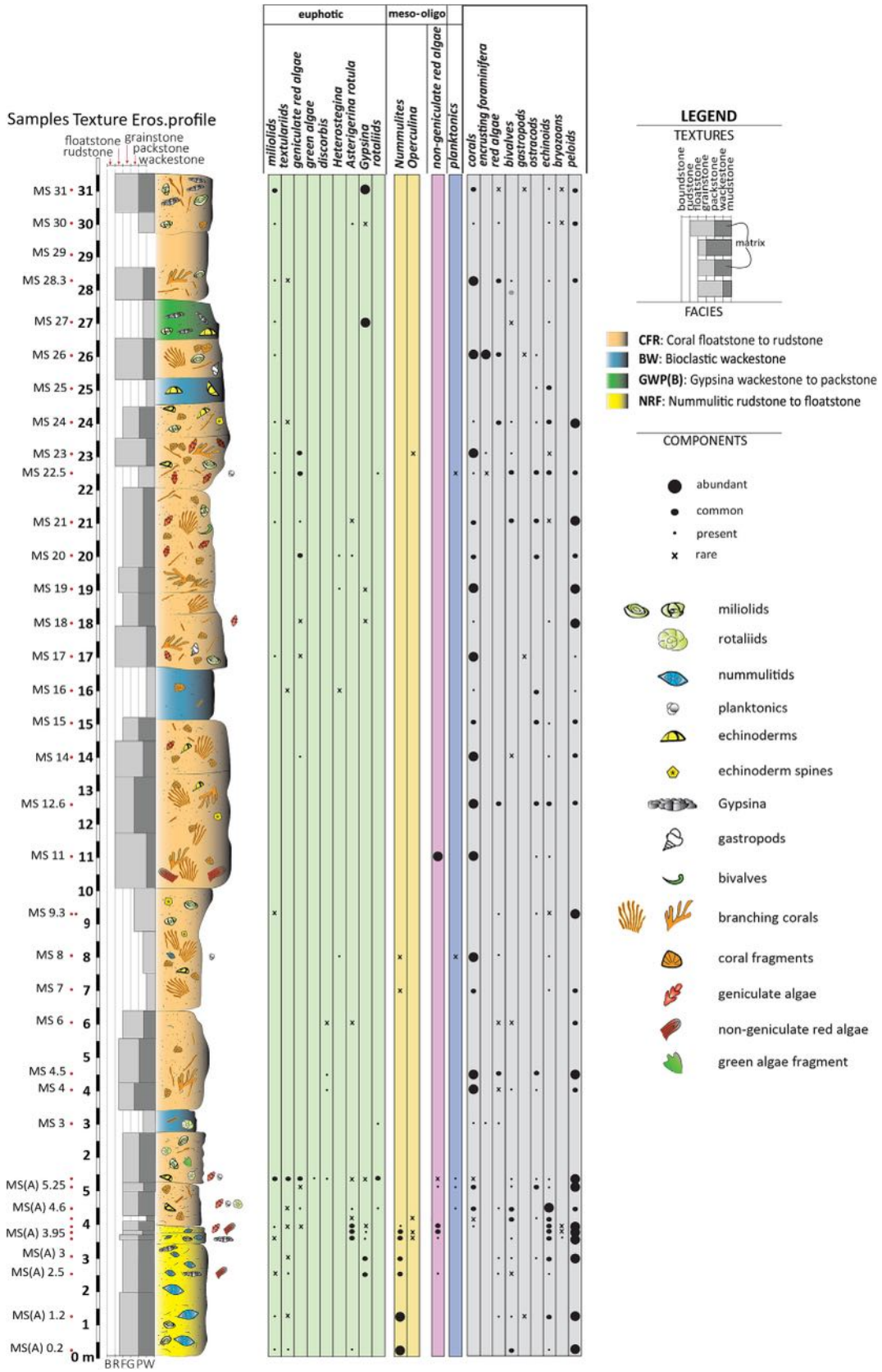

Fig. 7. Sedimentological and schematic log of the upper 31,5 m of the Monte Saraceno section inclusive of biostratigraphy. See text and Table 1 for lithofacies description.

either in size and abundance. This CIE interval, is marked by the first appearance of *Heterostegina* sp. and *Glomalveolina ungaroi*, and the lack of large nummulites in the upper interval of our study section. Moreover, the $\delta^{13}C$ and $\delta^{18}O$ values in the Monte Saraceno section show a significant positive correlation ($r^2 = 0.7$) (Fig. 10B).

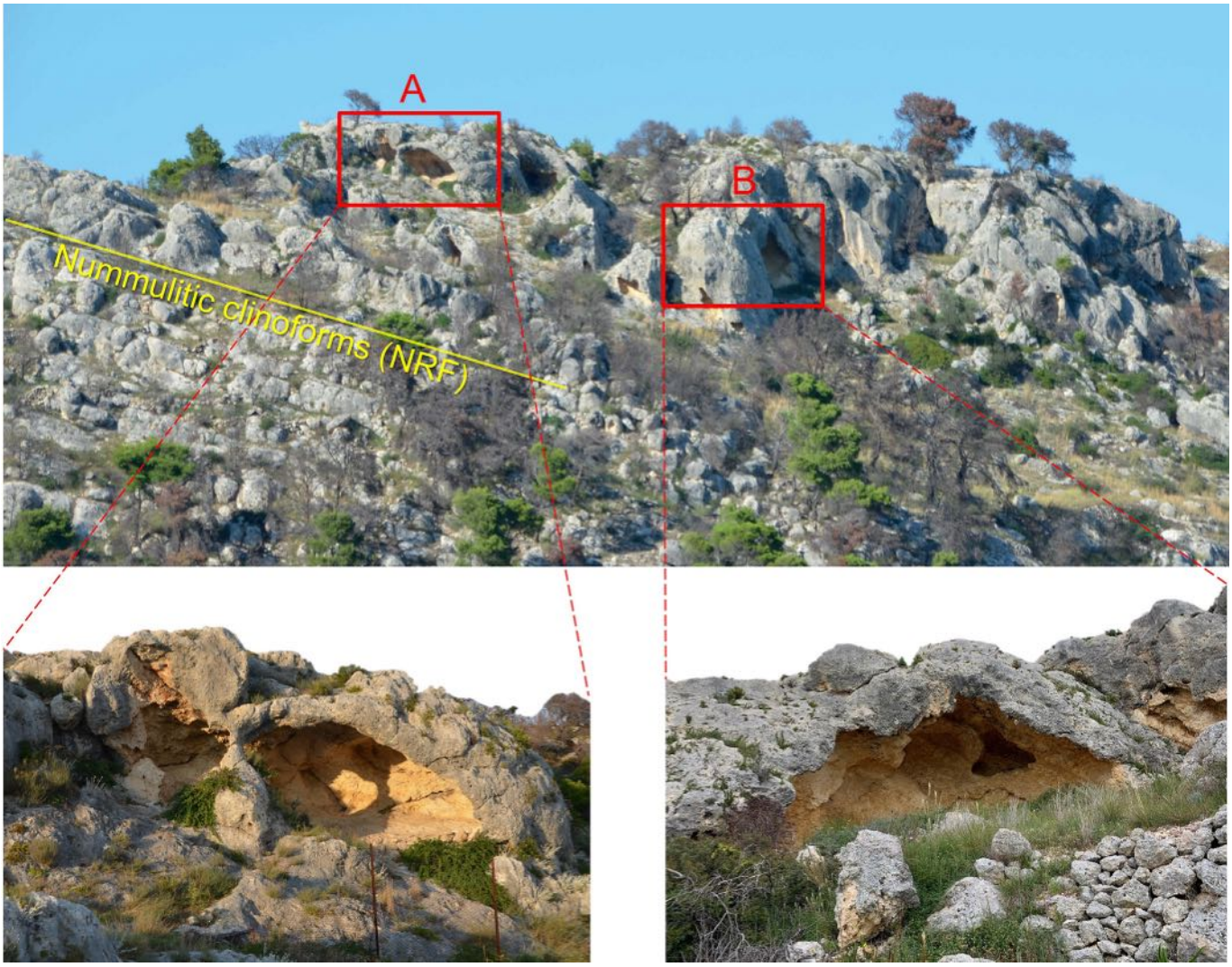

Fig. 8. Coral caves of the Monte Saraceno outcrop. Stratigraphically the caves are located respectively at 6 m and 12 m above the nummulites–corals facies shift.

5. Depositional model and carbonate factories

The Eocene shallow-water carbonate is usually depicted worldwide as typical ramp systems (sensu Burchette and Wright, 1992), in which the ramp is subdivided into an inner ramp (euphotic zone with seagrass dominated association), a mid ramp (meso-oligophotic zone with typical LBF association and other sciaphilic organisms) and an outer ramp (deep-oligophotic to aphotic zone) (Romero et al., 2002; Beavington-Penney and Racey, 2004; Nebelsick et al., 2005; Martín-Martín et al., 2021).

However, considering the carbonate platform geometries of this study, the palaeoenvironmental reconstruction of Monte Saraceno best fits with the non-rimmed shelf platform model (sensu Wilson, 1975; Read, 1985), or with a profile similar to a distally steepened ramp (Schlager, 2005, p. 64), rather than a classical Eocene homoclinal ramp-like system. Here, the euphotic outer shelf (inner ramp equivalent in terms of facies) and the slope and base-of-slope settings (mid to outer ramp equivalent) were observed. Within the slope, the occurrence of different LBF representing shallow to deep environments, allows us to divide it into proximal and distal.

Likewise, the foraminifera lifestyle and their functional morphology are useful factors for palaeoenvironmental and palaeoecological reconstruction. According to Hallock and Pomar (2009) and Mateu-Vicens et al. (2009), within the Nummulitidae and Amphisteginidae families, the shape changes relating to the light intensity. They present robust inflated forms in well illuminated, shallow-water settings becoming flatter and thinner with depth. Moreover, the texture, skeletal component analysis and the spatial distribution of the identified lithofacies, are essential to better reconstruct a realistic depositional model.

Our results suggest that the lithofacies of the Monte Saraceno Limestone span from distal slope to shallower settings, as the outer shelf with a probable seagrass meadow occurrence. In order to describe the two different types of carbonate factories with LBF and coral lithofacies, we propose two distinct depositional models (Fig. 11).

The clinoforms, rich in LBF, show a transition from a distal slope to an outer shelf setting. Here, the numerous occurrences of LBF (large flat *Nummulites* and *Discocyclina*) belonging to discocyclinid floatstone (DF) lithofacies are typical of a distal slope setting, below the chlorocline (meso-oligophotic zone). In the nummulitic rudstone to floatstone (NRF) lithofacies, the association of both flat and thick shape *Nummulites*, with porcelaneous foraminifera (miliolids), acervulinids (*Gypsina* hook-shaped), and rotaliids (*Gyroidinella magna*, *Asterigerina rotula*), indicates a proximal slope setting within the mesophotic zone. In this setting, the floatstone to rudstone textures indicate moderate and episodic hydrodynamic energy, able to rework skeletal sediments and transport ephiphytic foraminifera from shallower to deeper environments. In addition, going to the shallower zone, or outer shelf (euphotic zone), rare small and thick *Nummulites* associated with abundant hook-shaped acervulinids occurred (*Gypsina* wackestone to packstone lithofacies). According to Ungaro (1996), the hooked

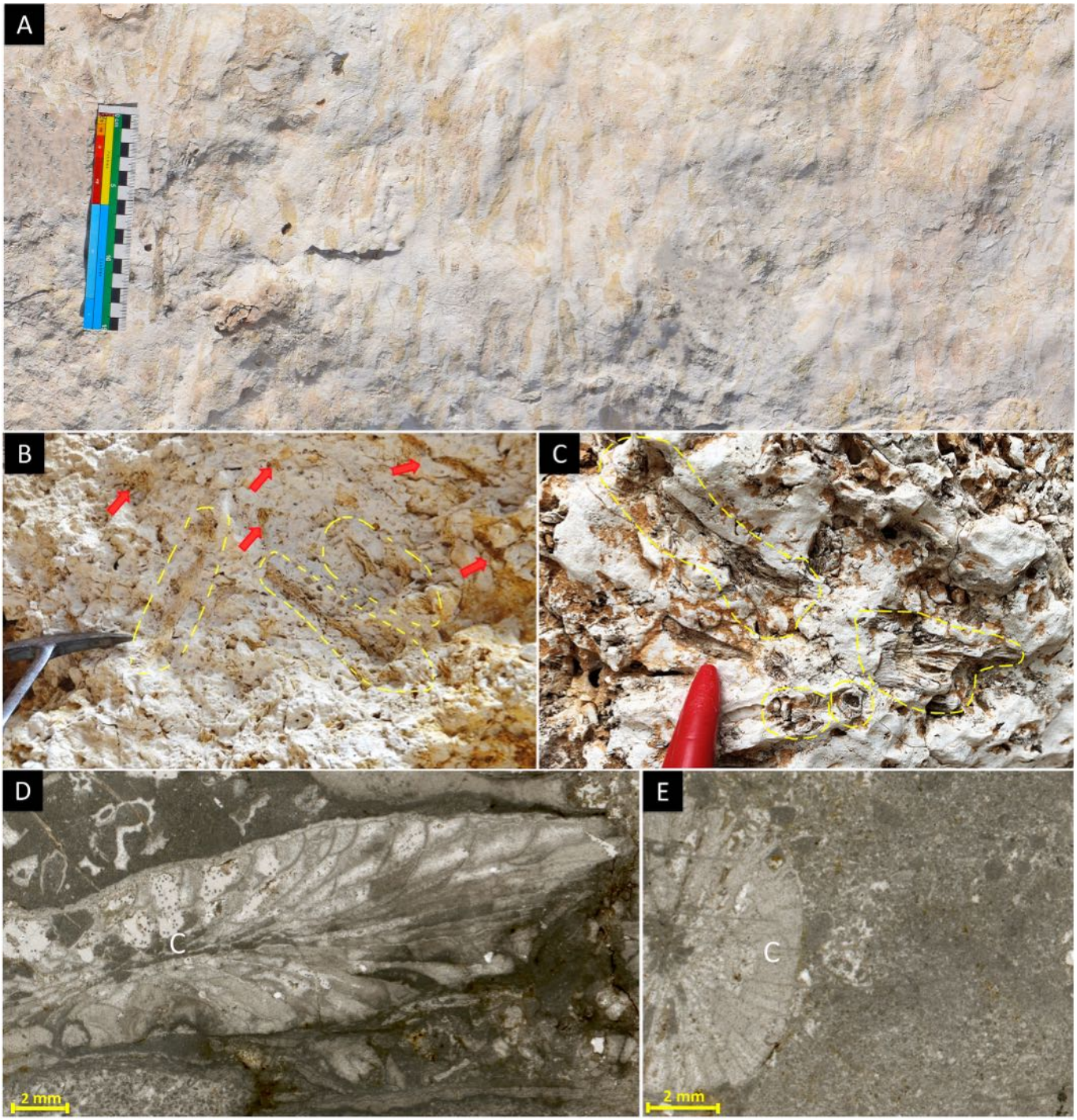

Fig. 9. A) Branching coral colony; B and C) detail of coral stick fragments inside the Monte Saraceno caves (yellow dotted lines and red arrows). Note the branching morphology of coral sticks immersed in a fine matrix (white); D and E) plane polarized thin section of branching coral fragments within a wackestone matrix (c = coral).

morphology represents an ephiphytic adaptation of the gypsinids attached to the edge of the seagrass leaves and it is considered a strong indicator of vegetated areas. This adaptation has been identified in the fossil record (e.g. Ungaro, 1996; Beavington-Penney et al., 2004) and in recent alveolinid fauna of the Caribbean as well (Eva, 1980). Furthermore, peloids, discorbids, and other seagrass indicators as *Sphaerogypsina globula*, *Planorbulina*, *Fabiania cassis*, *Gyroidinella magna*, and *Asterigerina rotula* could suggest the presence of seagrass meadows.

In the coral floatstone to rudstone (CFR) lithofacies, the association of coral fragments with shallow water components such as peloids, acervulinids (*Gypsina* sometimes hook-shaped), miliolids, small rotaliids and corallinaceean algae (*Lithoporella*) and, the minority of deeper skeletal association (small robust *Nummulites* and *Heterostegina*), strongly indicate a euphotic factory. The euphotic *Gypsina* wackestone to packstone (GWP) lithofacies is also interfingered with coral floatstone to rudstone (CFR), stratigraphically correspondent to the SBZ 18 (Fig. 11, B-model). This interfingering is directly visible in the outcrops adjacent to the coral rich-facies, where coral fragments are abundant with few *Nummulites*. Moreover, within the coral floatstone (CFR), the wackestone to packstone matrix texture would suggest a low-energy setting, maybe related to a baffling effect of the abundant

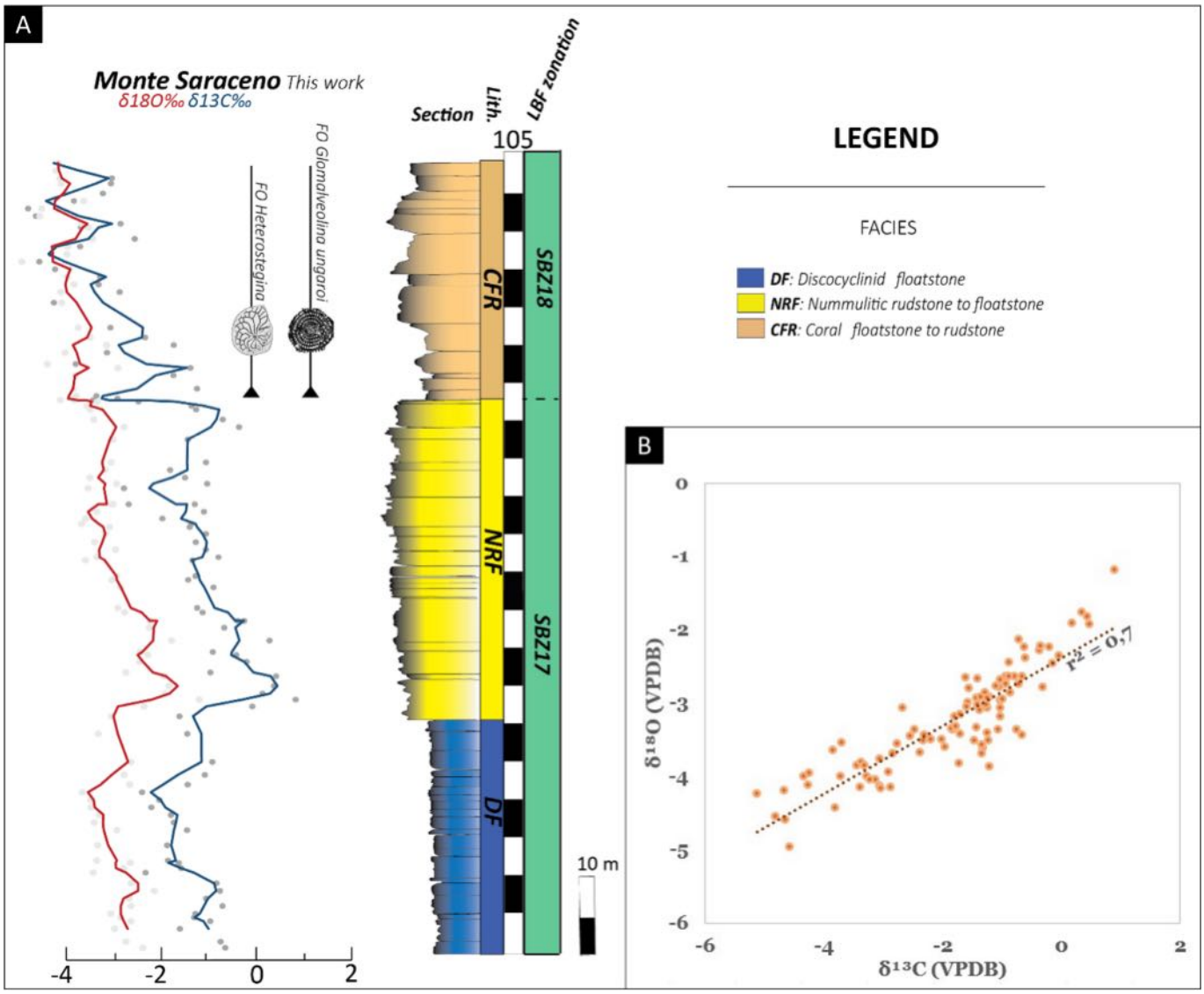

Fig. 10. A) Stable isotope results ($\delta^{18}O$, $\delta^{13}C$) and Shallow Benthic Zones (SBZs) of Monte Saraceno section. The Monte Saraceno isotopic curve is obtained from $\delta^{13}C$ and $\delta^{18}O$ values from lime mudstone portion of selected samples. The wide coloured lines correspond to the 3-point moving average. The SBZ 18 has been determined according to the appearance of the *Heterostegina* sp. and *Glomalveolina ungaroi*. See text and Table 1 for the lithofacies description. B) $\delta^{18}O$–$\delta^{13}C$ scatterplot of all Monte Saraceno samples. The regression lines are given for reference with the square correlation coefficients (r^2).

branching corals. Hence, the high concentration of coral fragments in the outcrop adjacent to the coral floatstone to rudstone (CFR) lithofacies and their absence in the small isolated outcrop, few tens of metres eastwards (see Fig. 3A), seem to suggest a patchy distribution of corals in the outer shelf setting (facies mosaic) and not a continuous and widespread shelf margin coral.

6. Discussion

6.1. The "nummulite bank" and slope cementation processes

The Monte Saraceno Limestone consists of a slope-to-basin succession in which prograding nummulitic clinoforms (NRF) are capped by a coral-rich facies (CRF). The clinoforms, with an average angle of 20° to 26°, pass tangentially basinwards to almost horizontal beds with some slide scar features (Adams et al., 2002). Considering the well exposed depositional geometries, it is possible to infer a relative "shallow" basin about 150 m deep. Moreover, Adams et al. (2002) showed that the linear slope profile of the Monte Saraceno clinoforms, which is directly correlated to grain size and texture, generally indicates deposition at or very close to the angle of repose. Compared to other middle Eocene examples that have typical ramp geometries (cfr. Beavington-Penney et al., 2005 and references therein), the Monte Saraceno nummulitic clinoforms show a very high angle of slope, thus not fitting in a classical ramp model. Hence, Guido et al. (2011) interpreted the Monte Saraceno clinoforms as a nummulite bank, demonstrating that this succession was interested by an intense microbial activity with in-situ production of automicrite that leads to a syndepositional cementation of the bank. Evidence of these activities is dense micritic masses, binding structures (Fig. 12A), peloidal texture (Fig. 12B-C), and clotted micrite patches (Fig. 12D). They considered the metabolic activity as the trigger mechanism allowing the precipitation of peloidal micrite between larger grains and consequently an early cementation of the clinoforms.

In this context we suggest that the unusual high angle of the Monte Saraceno slope, for such kind of deposits (i.e. nummulites banks and Eocene ramps), can be explained through a large nummulite production and deposition close to the angle of repose and a slope stabilization by binding and syndepositional cementation by microbial activities, that preserve the original angle and prevent further displacement of the nummulite tests.

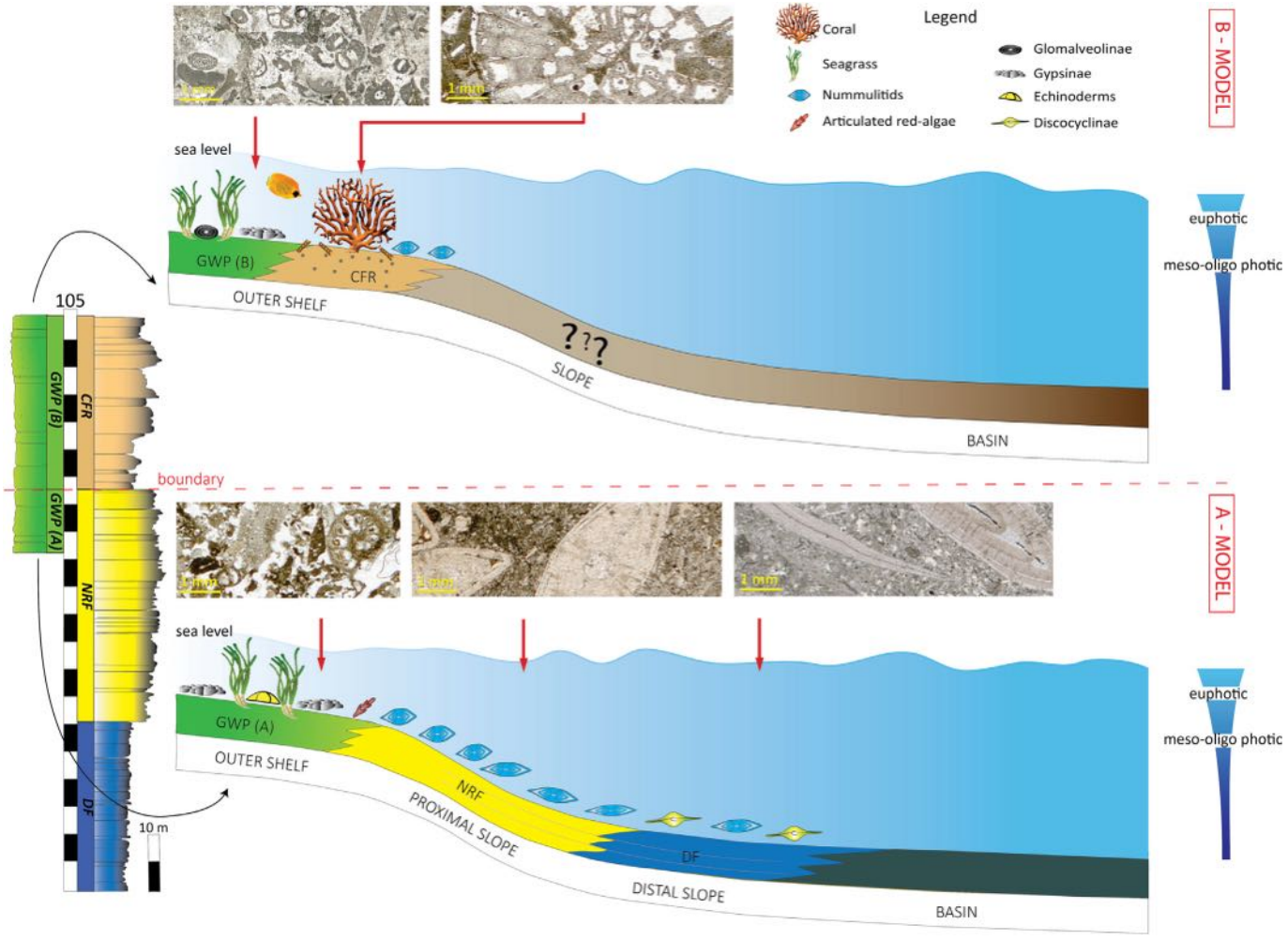

Fig. 11. Schematic section and depositional models of the investigated area. (A-MODEL) Nummulitic clinoform lithofacies represented by outer shelf (GWP(A)), proximal slope (NFR) and distal slope (DF) settings; (B-MODEL) coral interval consisting of GWP(B) and CFR lithofacies into an outer shelf setting. See text and Table 1 for the description of the lithofacies.

Similarly to Monte Saraceno, throughout the Earth's history, automicrites or microbialites have played a crucial role in carbonate platform and reefal environments (Reitner, 1993; Camoin et al., 1999).

During the Cenozoic, few carbonate slope examples stabilized by microbial activity have been studied. However, microbial stabilization of slopes has been identified as a significant factor in the late Miocene Cariatiz carbonate platform in SE Spain (Reolid et al., 2014) and in the Tongue of the Ocean in the Bahamas (Holocene) (Reolid et al., 2017). In this latter example, the slope angles exceed 35°, with Halimeda plates as a major constituent. These authors show that the occurrence of microbial binding prevented the slope failure by an early-stage (several tens of years) lithification, thus preserving the steep angles of the slope.

In Palaeozoic and Triassic platforms, carbonate slopes with angles steeper than 30° are attributed to stabilization processes involving organic framebuilding, microbial binding, and early lithification especially in their upper sections, compared to grain size (Kenter, 1990; Keim and Schlager, 1999, 2001; Della Porta et al., 2003, 2004; Kenter et al., 2005; Adams and Kenter, 2014). As a specific example, Marangon et al. (2011) studying the well-known Latemar platform (Triassic) describe an external margin and a steep slope (~35°) dominated by microbial products that formed and stabilized the slope sediments by trapping and bounding processes.

6.2. MECO and carbonate factory shift

Accurately determining the response of shallow-water carbonate factories to the Middle Eocene Climatic Optimum (MECO) on a global scale is a challenging task. To achieve a comprehensive understanding, it is crucial to integrate and compare high-resolution studies that focus on the stratigraphic, environmental, and ecological evolution of various carbonate systems spanning the middle Eocene age.

The Monte Saraceno outcrop represents an optimal scenario in which it is possible to infer the relationship between the carbonate factory shift and the climatic changes. In particular, although symbiotic organisms such as corals and LBF show similar ability to adapt to oligotrophic conditions (Hallock, 1988), they seem to react differently during warmer events (Martín-Martín et al., 2021; El-Azabi, 2023). The different genera that occurred in the studied succession, the LBF decreasing in size in the lower nummulitic interval and the *Heterostegina* sp. and *Glomalveolina ungaroi* FO in the upper coral facies, allows us to constrain the different sub-zones within this interval (SBZs 17–18). In the Monte Saraceno section, the lack of corals seems linked to the LBF flourishment and diversification during the MECO event (SBZ 17, sensu Papazzoni et al., 2017), confirming the unfavourable coral response compared to LBF. Here, LBF appear to be less sensitive to the temperature rise parameter decreasing in abundance and size going towards the following temperature drop (Fig. 13).

The significant changes in larger benthic foraminifera (LBF) assemblages occurred during the Middle to the Late Eocene, involving both extinctions and the first appearances of various lineages, enable us to identify the SBZs 17–18 within the studied interval. Specifically, during the Middle Eocene giant nummulitids of the genera *Nummulites* and *Assilina*, but also porcellanaeous foraminifera as alveolinids occurred.

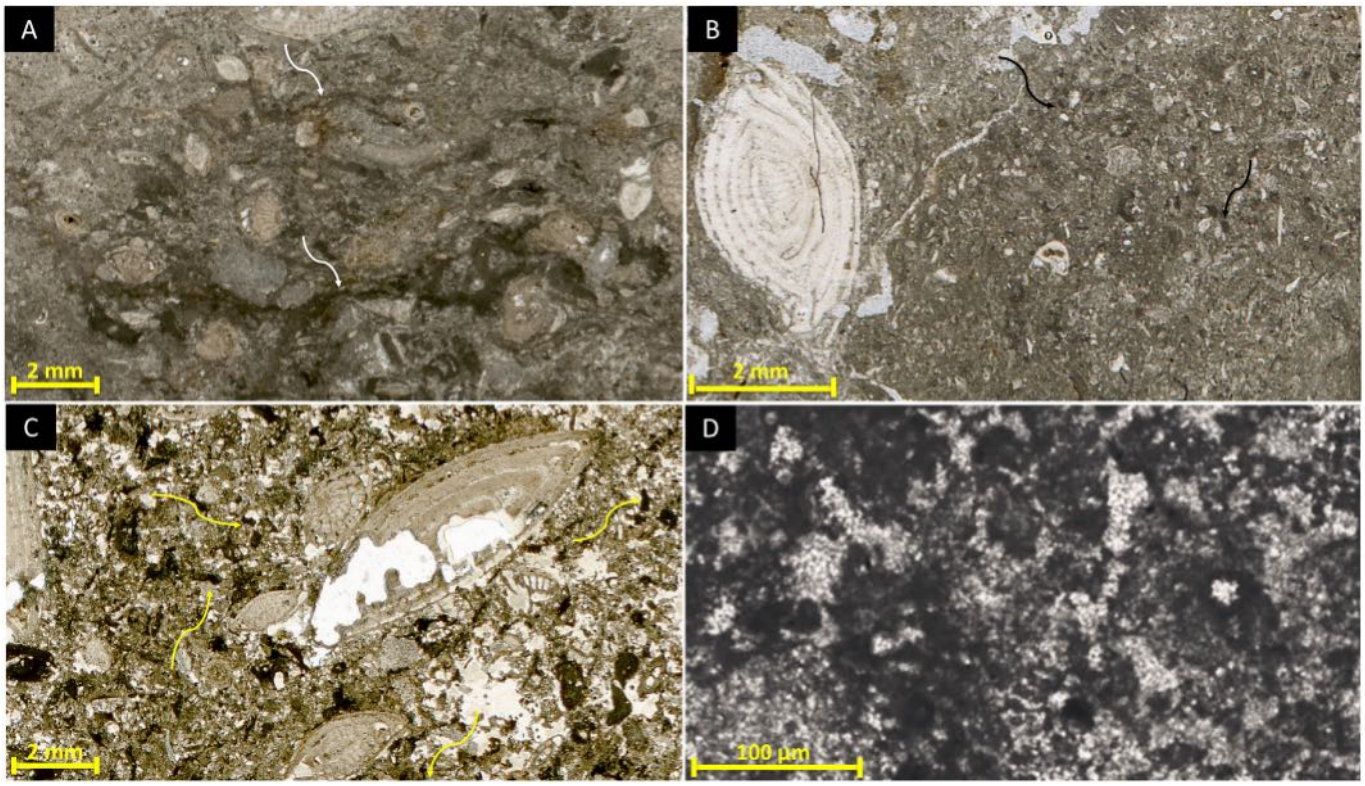

Fig. 12. A) Photomicrograph of a microbial binding (white arrow) with dense micrite connecting the different bioclasts; B and C) photomicrographs of a peloidal micrite in a nummulitic floatstone (black arrow); D) autochthonous clotted micrite patches with an antigravity fabric (Modified after Guido et al. (2011)).

Moreover, the Late Eocene was characterized by reticulate and small radiate *Nummulites*, nummulitids bearing secondary chamberlets such as *Heterostegina* and *Spiroclypeus* whilst, the early Oligocene, with a more restricted fauna containing only three small *Nummulites* and lacking

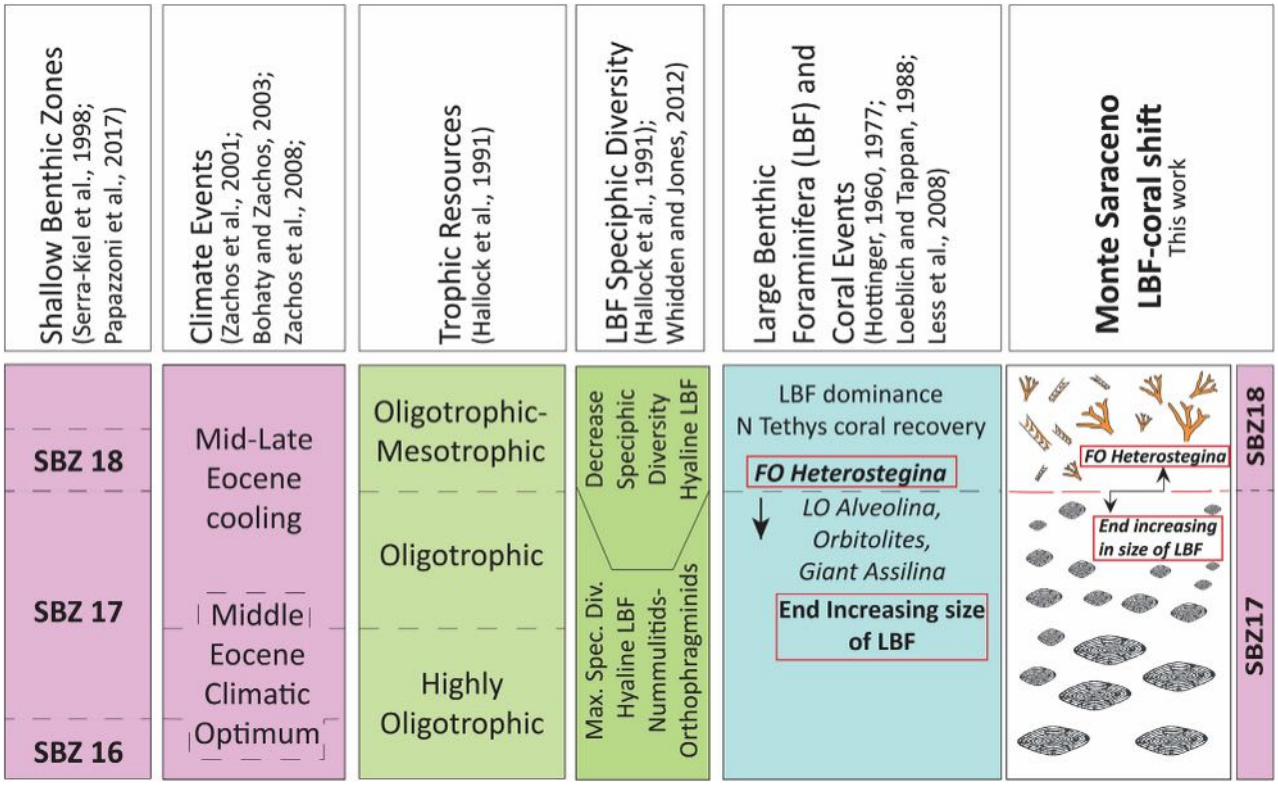

Fig. 13. Interpretations of main Eocene climatic events, trophic resource continuum, LBF specific diversity and coral events in the Tethyan domain are also illustrated (modified after Martín-Martín et al., 2023). Comparison between previous studies and Monte Saraceno highlighting the end of increasing in size of LBF and the *Heterostegina* sp. first occurrence in the LBF–coral facies shift.

orthophragmines and small *Assilina*. Moreover, during the post-MECO, the LBF assemblages also show significant changes with the local first and last occurrences of some LBF, in particular, the disappearance of alveolinids, and the initial dominance of *Heterostegina*, *Spiroclypeus*, the *Nummulites fabianii* group, *Pellatispira*, *Chapmanina*, and *Silvestriella* (Less and Özcan, 2012; Özcan et al., 2014, 2018). This LBF turnover, corresponding to significant bioevents in the Tethys, marks the SBZ 17–18 boundary (Papazzoni et al., 2017).

Late Palaeocene up to Lutetian examples of the Sierra Espuña–Mula Basin successions (Betic Cordillera, S Spain), the Moroccan Ghomarides Domain (Moroccan Internal Rif Zone) (Martín-Martín et al., 2020, 2021, 2023; Tosquella et al., 2022), and the Priabonian northern Italy successions (Nago Limestone) (Luciani, 1989; Bassi, 1998; Bosellini and Papazzoni, 2003), showed the co-existence of LBF and corals. Nevertheless, the LBF turnover and its relationship with the coral occurrence, have been demonstrated in several Mediterranean localities (e.g. Mossano section, Italy; Prebetic platform and Betic Cordillera, Spain; Maiella platform, Italy; Gavrovo–Tripolitza area, south Greece; Northern and Central Turkey; Tunisia; El-Ramliya area, Egypt). Specifically, the Gavrovo–Tripolitza area (southern continental Greece) and Maiella platform (Italy) corals' occurrence, as coral reefs, were dated as Priabonian although, during the early–middle Eocene, they were generally present but not as a major platform contributor as LBF (Moussavian and Vecsei, 1995; Vecsei and Moussavian, 1997; Barattolo et al., 2007). Likewise, Less et al. (2008) in the Mossano Section (Italy) supported the LBF turnover studying the change of co-occurring fossils such as the disappearance of large-sized *Nummulites*, followed by the appearance of the genus *Spiroclypeus* and by the disappearance of orthophragmines in the middle Eocene acme. In NW Turkey, the Thrace Basin during the Early Eocene was dominated by larger benthic foraminifera whilst the first coral reef appearance is dated as late Bartonian to Priabonian (Özcan et al., 2010; Less et al., 2011). Moreover, studies on the Prebetic platform (SE Spain) show that during the Eocene a great dominance of LBF and coralline red algae is coupled with a scarcity in corals until the Late Eocene, with a gradual decreasing of orthophragminids and nummulitids towards the upper part of the Middle Eocene succession. Hence, the corals' occurrence associated with the demise of many symbiont-bearing larger foraminifera in the northern and southern Tethyan realm, was related to the later global cooling event at the Bartonian–Priabonian boundary (Höntzsch et al., 2013). This is also reflected in the Sierra Espuña–Mula basin (Betic Cordillera, S-Spain), recently studied by Martín-Martín et al. (2021). They highlight the importance of the lower–upper Bartonian boundary (SBZs 17–18) as a critical scenario of biological change. In the Sierra Espuña–Mula basin, similarly to the Monte Saraceno section, the end of the increasing size of LBF tests, the last occurrence of *Alveolina*, *Orbitolites* and giant *Assilina* and the FO of the genus *Heterostegina* have been documented. Here, the marked reduction in specific diversity of hyaline LBF (nummulitids and orthophragminids) was related to an increase of trophism in the shallow-marine waters, which led to a reduction in the prevalence of LBF and a recovery of the zooxanthellate corals that gradually increase in size, number, and diversity (Martín-Martín et al., 2021). Similarly, Messaoud et al. (2023) in the Siouf Member (central Tunisia), integrating the abundance of microfossils, stable isotopes, and astrochronology, show that the maximum abundance of nummulites is linked to the MECO's warming peak. The hyperthermal event from 40.5 Ma to 39.8 Ma, in this area, was also correlated to a fast sea level rise, and associated mesotrophic condition, that promotes the formation of a shallow water carbonate platform. In the north Eastern Desert of Egypt, in the El-Ramliya area, the absence of the coral genus *Acropora* and the abundance of LBF were associated with the MECO hyperthermal event (El-Azabi, 2023). Specifically, the high nutrient levels, reached during this warm event, were considered detrimental for the coral growth (Hallock, 2000). Outside the Mediterranean Realm, the response of the shallow-water carbonate systems during the MECO event seems to follow the same pattern, with the flourishing of LBF (Khanolkar and Saraswati, 2019) and a reduction, or even the total absence of corals, which start to increase during the subsequent post-MECO cooling (Martín-Martín et al., 2021).

6.3. The isotopic variation across the Monte Saraceno section

Diagenetic, biological and physico-chemical processes can significantly influence the chemostratigraphy hiding the primary signal (Wendler, 2013). Oxygen isotopes present in carbonates are predominantly influenced by various factors, including the temperature during their formation, the mineral composition, the $\delta^{18}O$ value of the fluid responsible for carbonate precipitation ($\delta^{18}Ow$), pH, salinity, and more (Swart, 2015). However, $\delta^{18}O$ is often used as a proxy for temperature in marine environments (Fio et al., 2010). Conversely, carbon isotopes are more resistant to diagenetic processes (Schrag et al., 1995; Swart, 2015) although, mineralogy, kinetic effects and $\delta^{13}C$ signal from the dissolved organic carbon can influence $\delta^{13}C$ values (DIC; Wendler, 2013). The influx of factors such as carbonate material from outside the basin, terrestrial runoff, organic matter productivity, weathering, and burial rate, patterns of water circulation and stratification, as well as evaporation, can alter $\delta^{13}C$ values, mostly in proximal depositional environments (Saltzman and Thomas, 2012; Läuchli et al., 2021).

Thus, examining the correlation between $\delta^{13}C$ and $\delta^{18}O$ values is considered a fundamental method to evaluate the degree of diagenetic alteration (Brasier et al., 1996) in which, a significant positive correlation ($r^2 > 0.6$) suggests a diagenetic overprint of the primary isotopic signature (e.g. Fio et al., 2010). In this study, the $\delta^{13}C$ and $\delta^{18}O$ values in the Monte Saraceno section show a significant positive correlation ($r^2 = 0.7$) suggesting a diagenetic modification of the primary signal (Fig. 10B). Furthermore, the linear correlation in $\delta^{13}C$–$\delta^{18}O$ values suggests a mixing of two mineral end-members, specifically marine calcite and diagenetic calcite (Banner and Hanson, 1990).

The isotopically heavy end-members, with $\delta^{13}C$ values of around 0.7 ‰, come from samples mostly between 31 and 37 m, associated with the nummulitic flourishment within the nummulitic rudstone to floatstone (NRF) lithofacies, could be related to the peak of a warm climatic perturbation, the MECO event (Fig. 14). Conversely, the upper sharp negative CIE, associated with a shift to the coral facies and a reduction in size and abundance of *Nummulites* genus, could be a result of a simple lithofacies shift rather than the strong evidence of a temperature drop, the MECO-cooling. Moreover, the discocyclinid floatstone (DF), nummulitic rudstone to floatstone (NRF) and *Gypsina* wackestone to packstone (GWP(A)) lithofacies and the marked LBF decreasing in size before the transition to coral floatstone to rudstone (CFR) lithofacies (around 70 m), as well as the first occurrence (FO) of *Heterostegina* sp. and *Glomalveolina ungaroi* within the coral-rich (CFR) and *Gypsina* wackestone to packstone (GWP(B)) lithofacies, allow us to constrain the studied interval to the Shallow Benthic Zones (SBZs) 17–18. This enables us to compare the $\delta^{13}C$ shift to the stable isotope anomaly observed during the Middle Eocene Climatic Optimum (MECO) in various records, such as those from the Indian–Atlantic sector of the Southern Ocean (Bohaty and Zachos, 2003), the Contessa section (Jovane et al., 2007), and deep-sea sediments drilled during Ocean Drilling Program (ODP) and Integrated Ocean Drilling Program (IODP) expeditions (Cramer et al., 2009; Moebius et al., 2015; Henehan et al., 2020; Westerhold et al., 2020, among others).

Based on available proxy records, it is indicated that the Middle Eocene Climatic Optimum (MECO) greenhouse warming episode, around 40 million years ago, included approximately 400,000 years of gradual surface and deep ocean warming. This prolonged warming phase was followed by a short peak warming period, after which a relatively rapid cooling occurred over a span of approximately 100,000 years (Van der Ploeg et al., 2023). In addition, conversely to preceding early Eocene hyperthermals, as the PETM event (Zachos et al., 2010), the MECO is not marked by a contemporaneous negative $\delta^{13}C$ excursion, as also shown by the CIE of this study.

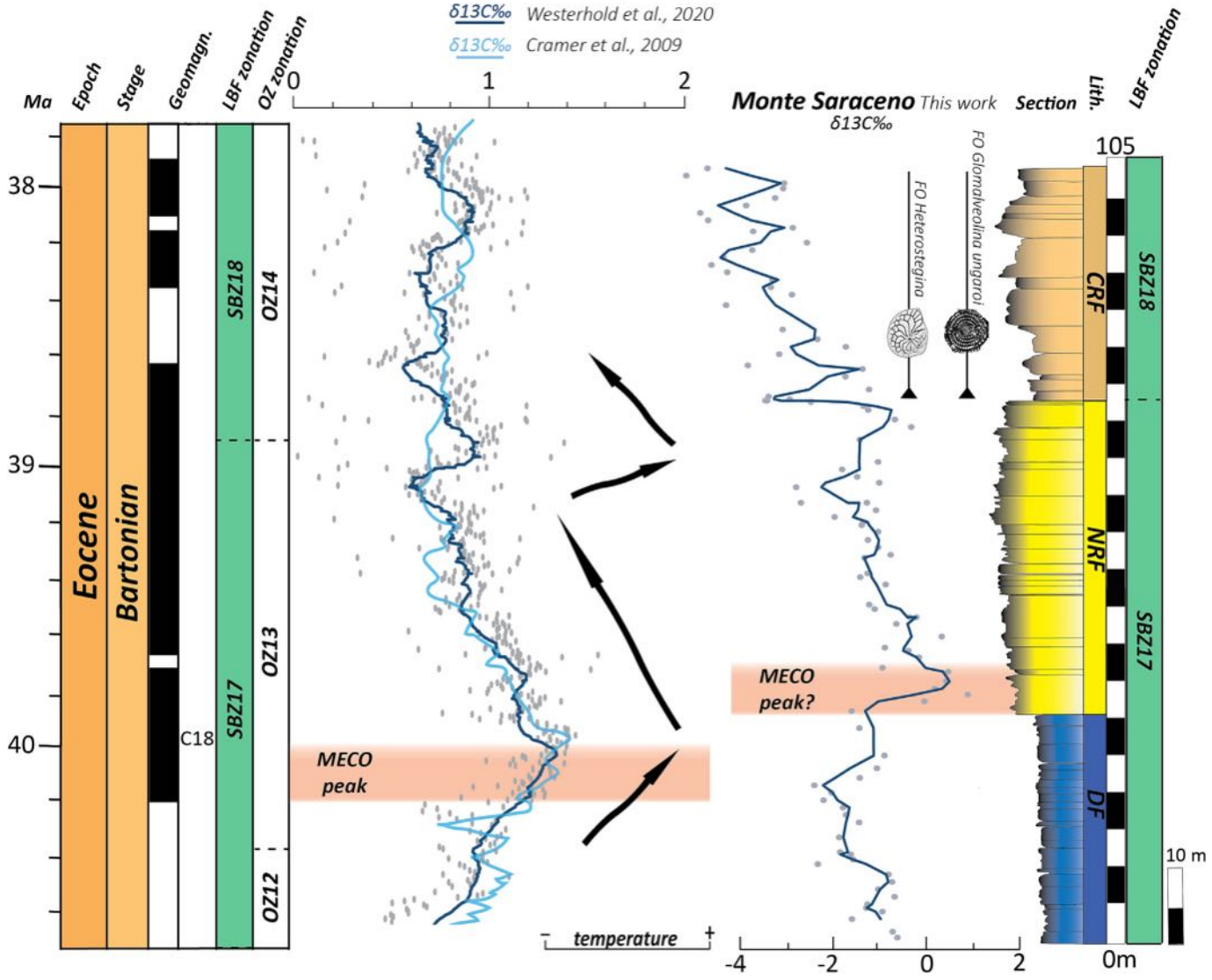

Fig. 14. Comparison of carbon isotope records and Shallow Benthic Zones (SBZs) between the Monte Saraceno section and Westerhold et al. (2020) and Cramer et al. (2009) datasets. The SBZ 18 has been associated with the *Heterostegina* sp. and *Glomalveolina ungaroi* first occurrence. See text and Table 1 for the description of the lithofacies.

7. Conclusions

The study of the palaeoenvironmental evolution of the Middle Eocene Monte Saraceno sequence, in the Apulia carbonate platform (Gargano Promontory, Southern Italy), highlights a sharp transition from a nummulite-dominated carbonate factory to a coral-rich interval. Thus, a detailed study of their distribution and evolution could be a useful key to identify short and long-term environmental changes in the shallow-water domain.

To obtain a reliable picture of the palaeoenvironment, a detailed identification of the skeletal components, integrated with isotopic analysis of stable isotope $\delta^{13}C$ and $\delta^{18}O$, was applied. Among the skeletal components, in order to identify the middle to late Eocene shallow benthic foraminiferal zones, LBF, mostly at the genus level were determined. In the Monte Saraceno outcrop, the lithofacies identification (NRF, DF, CFR, GWP(A-B), BW) allows us to reconstruct two different palaeoenvironmental models: i) A-model, attributed to the MECO event, characterized by the distal slope (discocyclinid floatstone (DF) lithofacies), proximal slope (nummulitic rudstone to floatstone (NRF) lithofacies) and outer shelf (*Gypsina* wackestone to packstone (GWP(A)) lithofacies); ii) B-model, assigned to the post-MECO cooling, represented by the upper coral facies (CFR) laterally intercalated with the *Gypsina* wackestone to packstone (GWP(B)) outer shelf lithofacies.

Additionally, the marked LBF decreasing in size just before the transition to the upper coral interval and the first occurrence (FO) of *Heterostegina* sp. and *Glomalveolina ungaroi* within the coral and acervulinid-rich (CRF and GWP(B)) lithofacies, can provide significant insights to constrain the studied interval within the Shallow Benthic Zones 17–18. In addition, the $\delta^{13}C$ and $\delta^{18}O$ values showing a significant positive correlation strongly suggest a diagenetic overprint and, more in detail, a mixing of two mineral endmembers, marine calcite and diagenetic calcite. Thus, we consider the positive $\delta^{13}C$ trend within the nummulitic-rich lithofacies (NRF) as possible evidence of the MECO event, contrary to the sharp negative shift moving upwards to the CFR lithofacies, probably associated with a simple facies shift.

In summary, we infer that the LBF–coral carbonate facies shift that occurred in the Monte Saraceno Limestone during the early–late Bartonian is strongly controlled by the MECO event. In particular, the calcitic larger foraminifera flourishment and lack of the aragonitic corals are related to the effects of the MECO warming. In contrast, the further post-MECO cooling represents favourable conditions for coral growth, as well documented during the onset of the icehouse period at the boundary between Eocene and Oligocene.

Hence, ancient shallow marine carbonate platforms and the various related carbonate facies, play a crucial role as valuable archives of past climate changes. These platforms, through their in situ biological deposition, provide a stratigraphic record of palaeoclimate documenting various physical variables within shallow marine environments, including circulation patterns, and sea level fluctuations and temperature.

In conclusion, the carbonate factory shift from a nummulite-dominated assemblage within the MECO hyperthermal event to a coral-dominated carbonate factory during the subsequent cooling phase highlights the sensitivity of carbonate ecosystems to evolving climatic conditions. These observations can be used in forecast models for the next global warming scenario.

CRediT authorship contribution statement

C. Morabito: Writing – review & editing, Writing – original draft, Visualization, Validation, Methodology, Investigation, Formal analysis, Data curation. **C.A. Papazzoni:** Writing – review & editing, Validation, Investigation, Data curation. **D.J. Lehrmann:** Writing – review & editing. **J.L. Payne:** Writing – review & editing, Validation, Funding acquisition. **K. Al-Ramadan:** Writing – review & editing, Funding acquisition. **M. Morsilli:** Writing – review & editing, Validation, Supervision, Resources, Project administration, Methodology, Investigation, Funding acquisition, Formal analysis, Data curation, Conceptualization.

Data availability

Isotopic dataset Monte Saraceno (Original data) (Mendeley Data)

Declaration of competing interest

The authors declare that they have no known competing financial interests or personal relationships that could have appeared to influence the work reported in this paper.

Acknowledgements

This work contributes to the project titled “Predictive Rules for the Development of Carbonate Platforms” (Subaward Agreement #61725381-125201) between Stanford University and the University of Ferrara (JP and MM). The project is supported by the College of Petroleum Engineering & Geosciences, King Fahd University of Petroleum and Minerals (KR).

Furthermore, this work is part of the project titled “Biota Resilience to Global Change: Biomineralization of Planktic and Benthic Calcifiers in the Past, Present, and Future” supported by MURST (PRIN 2017RX9XXXY-CM, MM).

Additionally, the research received partial support for MM and CM through funding provided by University of Ferrara1 (FAR 2020, 2021, and 2022) and IAS post-graduate research grants (2nd session 2020) for CM.

We acknowledge the Editor-in-Chief Catherine Chagué and the two anonymous reviewers for their relevant suggestions and comments which significantly improved the manuscript.

References

Adams, E.W., Kenter, J.A.M., 2014. So different, yet so similar: comparing and contrasting siliciclastic and carbonate slopes. In: Verwer, K., Playton, T.E., Harris, P.M. (Eds.), Deposits, Architecture and Controls of Carbonate Margin, Slope, and Basinal Settings. Society for Sedimentary Geology, Special Publicationvol. 105, pp. 14–25.

Adams, E.W., Morsilli, M., Schlager, W., Keim, L., Van Hoek, T., 2002. Quantifying the geometry and sediment fabric of linear slopes: examples from the Tertiary of Italy (Southern Alps and Gargano Promontory). Sedimentary Geology 154, 11–30.

Banner, J.L., Hanson, G.N., 1990. Calculation of simultaneous isotopic and trace element variations during water–rock interaction with applications to carbonate diagenesis. Geochimica et Cosmochimica Acta 54, 3123–3137.

Barattolo, F., Bassi, D., Romano, R., 2007. Upper Eocene larger foraminiferal–coralline algal facies from the Klokova Mountain (southern continental Greece). Facies 53, 361–375. https://doi.org/10.1007/s10347-007-0108-2.

Bassi, D., 1998. Coralline algal facies and their palaeoenvironments in the Late Eocene of Northern Italy (Calcare di Nago, Trento). Facies 39, 179–201. https://doi.org/10.1007/BF02537016.

Beavington-Penney, S.J., Racey, A., 2004. Ecology of extant nummulitids and other larger benthic foraminifera: applications in palaeoenvironmental analysis. Earth-Science Reviews 67, 219–265. https://doi.org/10.1016/j.earscirev.2004.02.005.

Beavington-Penney, S.J., Wright, V.P., Woelkerling, W.J., 2004. Recognising macrophyte vegetated environments in the rock record: a new criterion using ‘hooked’ forms of crustose coralline red algae. Sedimentary Geology 166, 1–9.

Beavington-Penney, S.J., Wright, V.P., Racey, A., 2005. Sediment production and dispersal on foraminifera-dominated early Tertiary ramps: the Eocene El Garia Formation, Tunisia. Sedimentology 52, 537–569. https://doi.org/10.1111/j.1365-3091.2005.00709.

Bertotti, G., Casolari, E., Picotti, V., 1999. The Gargano Promontory: a Neogene contractional belt within the Adriatic plate. Terra Nova 11, 168–173.

Bijl, P.K., Houben, A.J.P., Schouten, S., Bohaty, S.M., Sluijs, A., Reichart, G.J., Sinninghe Damsté, J.S., Brinkhuis, H., 2010. Transient Middle Eocene atmospheric CO_2 and temperature variations. Science 330, 819–821.

Bohaty, S.M., Zachos, J.C., 2003. Significant Southern Ocean warming event in the late middle Eocene. Geology 31, 1017–1020.

Bohaty, S.M., Zachos, J.C., Florindo, F., Delaney, M.L., 2009. Coupled greenhouse warming and deep-sea acidification in the middle Eocene. Paleoceanography and Paleoclimatology 24, PA2207. https://doi.org/10.1029/2008PA001676.

Borgomano, J.R.F., 2000. The Upper Cretaceous carbonates of the Gargano–Murge region, southern Italy: a model of platform-to-basin transition. AAPG Bullettin 84, 1561–1588.

Boscolo Galazzo, F., Giusberti, L., Luciani, V., Thomas, E., 2013. Paleoenvironmental changes during the Middle Eocene Climatic Optimum (MECO) and its aftermath: the benthic foraminiferal record from the Alano section (NE Italy). Palaeogeography, Palaeoclimatology, Palaeoecology 378, 22–35. https://doi.org/10.1016/j.palaeo.2013.03.018.

Bosellini, A., Neri, C., 1995. L'Eocene di Monte Saraceno (Promontorio del Gargano, Puglia). Annali Università di Ferrara (N.S.), Sezione Scienze della Terra 6, 27–40.

Bosellini, F., Papazzoni, C., 2003. Palaeoecological significance of coral-encrusting foraminiferan associations: a case-study from the Upper Eocene of northern Italy. Acta Palaeontologica Polonica 48, 279–292.

Bosellini, A., Neri, C., Luciani, V., 1993. Platform margin collapses and sequence stratigraphic organisation of carbonate slopes: Cretaceous–Eocene, Gargano Promontory, southern Italy. Terra Nova 5, 282–297.

Bosellini, A., Morsilli, M., Neri, C., 1999. Long-term event stratigraphy of the Apulia Platform Margin (Upper Jurassic To Eocene, Gargano, Southern Italy). Journal of Sedimentary Research 69, 1241–1252. https://doi.org/10.1306/D4268B4E-2B26-11D7-8648000102C1865D.

Brankman, C., Aydin, A., 2004. Uplift and contractional deformation along a segmented strike-slip fault system: the Gargano Promontory, southern Italy. Journal of Structural Geology 26, 807–824. https://doi.org/10.1016/j.jsg.2003.08.018.

Brasier, M.D., Shields, G., Kuleshov, V.N., Zhegallo, E.A., 1996. Integrated chemo-and biostratigraphic calibration of early animal evolution: Neoproterozoic–early Cambrian of southwest Mongolia. Geological Magazine 133, 445–485. https://doi.org/10.1017/S0016756800007603.

Burchette, T.P., Wright, V.P., 1992. Carbonate ramp depositional systems. Sedimentary Geology 79, 3–57.

Camoin, G.F., Gautret, P., Montaggioni, L.F., Cabioch, G., 1999. Nature and environmental significance of microbia-lites in Quaternary reefs: the Tahiti paradox. Sedimentary Geology 126, 271–304.

Cramer, B.S., Toggweiler, J.R., Wright, J.D., Katz, M.E., Miller, K.G., 2009. Ocean overturning since the Late Cretaceous: inferences from a new benthic foraminiferal isotope compilation. Paleoceanography 24, PA4216. https://doi.org/10.1029/2008PA001683.

Cramwinckel, M.J., Huber, M., Kocken, I.J., Agnini, C., Bijl, P.K., Bohaty, S.M., Frieling, J., Goldner, A., Hilgen, F.J., Kip, E.L., Peterse, F., Van Der Ploeg, R., Röhl, U., Schouten, S., Sluijs, A., 2018. Synchronous tropical and polar temperature evolution in the Eocene letter. Nature 559, 382–386. https://doi.org/10.1038/s41586-018-0272-2.

De Alteriis, G., Aiello, G., 1993. Stratigraphy and tectonics offshore of Puglia (Italy, southern Adriatic Sea). Marine Geology 113, 233–253.

Della Porta, G., Kenter, J.A.M., Bahamonde, J.R., Immenhauser, A., Villa, E., 2003. Microbial boundstone dominated carbonate slope (Upper Carboniferous, N Spain): microfacies, lithofacies distribution and stratal geometry. Facies 49, 175–208.

Della Porta, G., Kenter, J.A.M., Bahamonde, J.R., 2004. Depositional facies and stratal geometry of an Upper Carboniferous prograding and aggrading high-relief carbonate platform (Cantabrian Mountains, N Spain). Sedimentology 51, 267–295.

Doglioni, C., Mongelli, F., Pieri, P., 1994. The Puglia uplift (SE Italy). An anomaly in the foreland of the Apenninic subduction due to buckling of a thick continental lithosphere. Tectonics 13, 1309–1321.

Dunham, R.J., 1962. Classification of carbonate rocks according to their depositional texture. In: Ham, W.E. (Ed.), Classification of Carbonate Rocks. American Association of Petroleum Geologists Memoirvol. 1, pp. 108–121.

Eberli, G.P., Bernoulli, D., Sanders, D., Vecsei, A., 1993. From aggradation to progradation: the Maiella Platform, Abruzzi, Italy. In: Simo, T., Scott, R.W., Masse, J.P. (Eds.), Cretaceous Carbonate Platforms. American Association of Petroleum Geologists Memoirvol. 56, pp. 213–232.

Edgar, K.M., Wilson, P.A., Sexton, P.F., Gibbs, S.J., Roberts, A.P., Norris, R.D., 2010. New biostratigraphic, magnetostratigraphic and isotopic insights into the Middle Eocene

Climatic Optimum in low latitudes. Palaeogeography, Palaeoclimatology, Palaeoecology 297, 670–682. https://doi.org/10.1016/j.palaeo.2010.09.016.
El-Azabi, H.M., 2023. Sedimentary facies and stratal architecture of the Middle Eocene Acropora-dominated succession in a storm-influenced ramp system, El-Ramliya area, north Eastern Desert, Egypt. Sedimentary Geology 447, 106368. https://doi.org/10.1016/j.sedgeo.2023.106368.
Eva, A.N., 1980. Pre-Miocene seagrass communities in the Caribbean. Palaeontology 23, 231–236.
Fio, K., Spangenberg, J.E., Vlahović, I., Sremac, J., Velić, I., Mrinjek, E., 2010. Stable isotope and trace element stratigraphy across the Permian–Triassic transition: a redefinition of the boundary in the Velebit Mountain, Croatia. Chemical Geology 278, 38–57. https://doi.org/10.1016/j.chemgeo.2010.09.001.
Giorgioni, M., Jovane, L., Rego, E.S., Rodelli, D., Frontalini, F., Coccioni, R., Catanzariti, R., Özcan, E., 2019. Carbon cycle instability and orbital forcing during the Middle Eocene Climatic Optimum. Scientific Reports 9. https://doi.org/10.1038/s41598-019-45763-2.
Gooday, A.J., 2003. Benthic foraminifera (Protista) as tools in deep-water palaeoceanography: a review of environmental influences on faunal characteristics. Advances in Marine Biology 46, 1–90. https://doi.org/10.1016/S0065-2881(03)46002-1.
Guido, A., Papazzoni, C.A., Mastandrea, A., Morsilli, M., La Russa, M.F., Tosti, F., Russo, F., 2011. Automicrite in a "nummulite bank" from the Monte Saraceno (Southern Italy): evidence for synsedimentary cementation. Sedimentology 58, 878–889. https://doi.org/10.1111/j.1365-3091.2010.01187.x.
Hallock, P., 1985. Why are larger Foraminifera large? Paleobiology 11, 195–208.
Hallock, P., 1988. Diversification in algal symbiont-bearing foraminifera: a response to oligotrophy. Revue de Paléobiologie Special volume 2 (Benthos '86), 789–797.
Hallock, P., 2000. Symbiont-bearing foraminifera: harbingers of global change? Micropaleontology 46, 95–104.
Hallock, P., Pomar, L., 2009. Cenozoic evolution of larger benthic foraminifers: paleoceanographic evidence for changing habitats. Proceedings of the 11th International Coral Reef Symposium Ft. Lauderdale, Florida, pp. 16–20.
Henehan, M.J., Edgar, K.M., Foster, G.L., Penman, D.E., Hull, P.M., Greenop, R., Anagnostou, E., Pearson, P.N., 2020. Revisiting the Middle Eocene Climatic Optimum "carbon cycle conundrum" with new estimates of atmospheric pCO_2 from boron isotopes. Paleoceanography and Paleoclimatology 35. https://doi.org/10.1029/2019PA003713.
Höntzsch, S., Scheibner, C., Guasti, E., Kuss, J., Marzouk, A.M., Rasser, M., 2011. Increasing restriction of the Egyptian shelf during the Early Eocene? New insights from a southern Tethyan carbonate platform. Palaegeography, Palaeoclimatology, Palaeoecology 302, 349–366.
Höntzsch, S., Scheibner, C., Brock, J.P., Kuss, J., 2013. Circum-Tethyan carbonate platform evolution during the Palaeogene: the Prebetic platform as a test for climatically controlled facies shifts. Turkish Journal of Earth Sciences 22, 891–918. https://doi.org/10.3906/yer-1207-8.
Hottinger, L., 1983. Processes determining the distribution of larger foraminifera in space and time. Utrecht Micropaleontology Bulletin 30, 239–253.
Hottinger, L., 1998. Shallow benthic foraminifera at the Paleocene–Eocene boundary. Strata 9, 61–64.
Hottinger, L., 2001. Learning from the past? In: Box, E., Pignatti, S. (Eds.), Volume IV, The Living World. Part Two. Academic Press, San Diego, USA, pp. 449–477
Insalaco, E., 1998. The descriptive nomenclature and classification of growth fabrics in fossil scleractinian reefs. Sedimentary Geology 118, 159–186. https://doi.org/10.1016/S0037-0738(98)00011-6.
Jovane, L., Florindo, F., Coccioni, R., Dinarès-Turell, J., Marsili, A., Monechi, S., Roberts, A.P., Sprovieri, M., 2007. The middle Eocene climatic optimum event in the Contessa Highway section, Umbrian Apennines, Italy. Bulletin of the Geological Society of America 119, 413–427. https://doi.org/10.1130/B25917.1.
Keim, L., Schlager, W., 1999. Automicrite facies on steep slopes (Triassic, Dolomites, Italy). Facies 41, 15–25.
Keim, L., Schlager, W., 2001. Quantitative compositional analysis of a Triassic carbonate platform (Southern Alps, Italy). Sedimentary Geology 139, 261–283.
Kenter, J.A.M., 1990. Carbonate platform flanks: slope angle and sediment fabric. Sedimentology 72, 777–794.
Kenter, J.A.M., Harris, P.M., Della Porta, G., 2005. Steep microbial boundstonedominated platform margins: examples and implications. Sedimentary Geology 178, 5–30.
Khanolkar, S., Saraswati, P.K., 2019. Eocene foraminiferal biofacies in Kutch Basin (India) in context of palaeoclimate and palaeoecology. Journal of Palaeogeography 8, 21. https://doi.org/10.1186/s42501-019-0038-2.
Khanolkar, S., Saraswati, P.K., Rogers, K., 2017. Ecology of foraminifera during the middle Eocene climatic optimum in Kutch, India. Geodinamica Acta 29, 181–193. https://doi.org/10.1080/09853111.2017.1300846.
Langer, M.R., 2008. Assessing the contribution of foraminiferan protists to global ocean carbonate production. Journal of Eukaryotic Microbiology 55, 163–169. https://doi.org/10.1111/j.1550-7408.2008.00321.x.
Läuchli, C., Garcés, M., Beamud, E., Valero, L., Honegger, L., Adatte, T., Castelltort, S., 2021. Magnetostratigraphy and stable isotope stratigraphy of the middle-Eocene succession of the Ainsa basin (Spain): new age constraints and implications for sediment delivery to the deep waters. Marine and Petroleum Geology 132, 105182. https://doi.org/10.1016/j.marpetgeo.2021.105182.
Less, G., Özcan, E., 2012. Bartonian-Priabonian larger benthic foraminiferal events in the Western Tethys. Austrian Journal of Earth Sciences 105, 129–140.
Less, G., Özcan, E., Papazzoni, C.A., Stockar, R., 2008. Middle to late Eocene evolution of nummulitid foraminifer *Heterostegina* in the Western Tethys. Acta Palaeontologica Polonica 53, 317–350. https://doi.org/10.4202/app.2008.0212.
Less, G., Özcan, E., Okay, A.I., 2011. Stratigraphy and larger foraminifera of the middle eocene to lower oligocene shallow-marine units in the northern and eastern parts of the trace basin, NW Turkey. Turkish Journal of Earth Sciences 20, 793–845. https://doi.org/10.3906/yer-1010-53.
Luciani, V., 1989. Stratigrafia sequenziale del terziario nella catena del Monte Baldo (Province di Verona e Trento). Memorie di Scienze Geologiche 41, 263–351.
Luciani, V., Giusberti, L., Agnini, C., Fornaciari, E., Rio, D., Boscorth, D.J.A., Pälike, H., 2010. Ecological and evolutionary response of Tethyan planktonic foraminifera to the middle Eocene climatic optimum (MECO) from the Alano section (NE Italy). Palaeogeography, Palaeoclimatology, Palaeoecology 292, 82–95. https://doi.org/10.1016/j.palaeo.2010.03.029.
Marangon, A., Gattolin, G., Della Porta, G., Preto, N., 2011. The Latemar: a flat-topped, steep fronted platform dominated by microbialites and synsedimentary cements. Sedimentary Geology 240, 97–114. https://doi.org/10.1016/j.sedgeo.2011.09.001.
Martín-Martín, M., Guerrera, F., Tosquella, J., Tramontana, M., 2020. Paleocene–Lower Eocene carbonate platforms of westernmost Tethys. Sedimentary Geology 404, 105674. https://doi.org/10.1016/j.sedgeo.2020.105674.
Martín-Martín, M., Guerrera, F., Tosquella, J., Tramontana, M., 2021. Middle Eocene carbonate platforms of the westernmost Tethys. Sedimentary Geology 415, 105861. https://doi.org/10.1016/j.sedgeo.2021.105861.
Martín-Martín, M., Tosquella, J., Guerrera, F., Maaté, A., Hlila, R., Maaté, S., Tramontana, M., Le Breton, E., 2023. The Eocene carbonate platforms of the Ghomaride Domain (Internal Rif Zone, N Morocco): a segment of the westernmost Tethys. Sedimentary Geology 452, 106423. https://doi.org/10.1016/j.sedgeo.2023.106423.
Mateu-Vicens, G., Hallock, P., Brandano, M., 2009. Test shape variability of Amphistegina d'Orbigny 1826 as a paleobathymetric proxy: application to two Miocene examples. In: Demchuk, T., Gary, A. (Eds.), Geologic Problems Solving With Microfossils. SEPM Special Publicationvol. 93, pp. 67–82.
Matteucci, R., 1971. Revisione di alcuni Nummuliti significativi dell'Eocene del Gargano (Puglia). Geologica Romana 9, 205–238.
Matteucci, R., 1978. Foraminiferi epibionti e criptobionti in gusci di Nummuliti dell'Eocene medio del Gargano (Puglia). Geologica Romana 17, 389–410.
Matteucci, R., Pignatti, J., Di Carlo, M., Ragusa, M., 2012. Le facies a macroforaminiferi del Paleocene-Eocene del Gargano meridionale. In: Zunino, M., et al. (Eds.), Gargano, un archivio della diversità geologica dal Mesozoico al Pleistocene. Giornate di Paleontologia, IX Edizione - Apricena, 2009. Geol. Field Trips, pp. 32–39 https://doi.org/10.3301/GFT.2012.02.
Messaoud, J.H., Thibault, N., De Vleeschouwer, D., Monkenbusch, J., 2023. Benthic biota (nummulites) response to a hyperthermal event: eccentricity-modulated precession control on climate during the middle Eocene warming in the Southern Mediterranean. Palaeogeography, Palaeoclimatology, Palaeoecology 626, 111712. https://doi.org/10.1016/j.palaeo.2023.111712.
Moebius, I., Friedrich, O., Edgar, K.M., Sexton, P.F., 2015. Episodes of intensified biological productivity in the subtropical Atlantic Ocean during the termination of the Middle Eocene Climatic Optimum (MECO). Paleoceanography and Paleoclimatology 30, 1041–1058.
Morsilli, M., Bosellini, A., 1997. Carbonate facies zonation of the Upper Jurassic–Lower Cretaceous Apulia Platform Margin. Rivista Italiana di Paleontologia e Stratigrafia 103, 193–206. https://doi.org/10.13130/2039-4942/5290.
Morsilli, M., Rusciadelli, G., Bosellini, A., 2004. The Apulia carbonate platform margin and slope, Late Jurassic to Eocene of the Maiella and Gargano Promontory: physical stratigraphy and architecture. Field Trip Guide Book. 32nd International Geological Congress, 20–28 August 2004, Florence, Italy, pp. 1–44.
Morsilli, M., Hairabian, A., Borgomano, J., Nardon, S., Adams, E.W., Gartner, G.B., 2017. The Apulia Carbonate platform—Gargano Promontory, Italy (Upper Jurassic–Eocene). AAPG Bulletin 101, 523–531. https://doi.org/10.1306/011817DIG17031.
Morsilli, M., Hairabian, A., Borgomano, J., Nardon, S., Adams, E.W., Bracco Gartner, G.B., 2021. A journey along the Gargano Promontory (Southern Italy): the Late Jurassic to Eocene Apulia Carbonate Platform evolution. In: Wright, V.P., Della Porta, G. (Eds.), Field Guides to Exceptionally Exposed Carbonate Outcrops. International Association of Sedimentologists Field Guides, pp. 395–480.
Moussavian, E., Vecsei, A., 1995. Paleocene reef sediments from the Maiella carbonate platform, Italy. Facies 32, 213–222.
Murray, J.W., 2006. Ecology and Applications of Benthic Foraminifera. Cambridge University Press, p. 426.
Nebelsick, J.H., Rasser, M.W., Bassi, D., 2005. Facies dynamics in Eocene to Oligocenecircumalpine carbonates. Facies 51, 197–217.
Özcan, E., Less, G., Okay, A.I., Báldi-Beke, M., Kollányi, K., Ömer Yilmaz, I., 2010. Stratigraphy and larger foraminifera of the eocene shallow-marine and olistostromal units of the Southern Part of the Thrace Basin, NW Turkey. Turkish Journal of Earth Sciences 19, 27–77. https://doi.org/10.3906/yer-0902-11.
Özcan, E., Scheibner, C., Boukhalfa, K., 2014. Orthophragminids (foraminifera) across the Paleocene–Eocene transition from North Africa: taxonomy, biostratigraphy, and paleobiogeographic implications. Journal of Foraminiferal Research 44, 203–229. https://doi.org/10.2113/gsjfr.44.3.203.
Özcan, E., Okay, A.I., Bürkan, K.A., Yücel, A.O., Özcan, Z., 2018. Middle–late eocene marine record of the Biga Peninsula, NW Anatolia, Turkey. Geologica Acta 16, 163–187. https://doi.org/10.1344/GeologicaActa2018.16.2.4.
Papazzoni, C., Cosovic, V., Briguglio, A., Drobne, K., 2017. Towards a calibrated Larger Foraminifera biostratigraphic zonation: celebrating 18 years of the application of Shallow Benthic Zones. Palaios 32, 1–5.
Pomar, L., Bassant, P., Brandano, M., Ruchonnet, C., Janson, X., 2012. Impact of carbonate producing biota on platform architecture: insights from Miocene examples of the Mediterranean region. Earth-Science Reviews 113, 186–211. https://doi.org/10.1016/j.earscirev.2012.03.007.
Pomar, L., Baceta, J., Hallock, P., Mateu-Vicens, G., Basso, D., 2017. Reef building and carbonate production modes in the west-central Tethys during the Cenozoic. Marine

and Petroleum Geology 83, 261–304. https://doi.org/10.1016/j.marpetgeo.2017.03.015.
Read, J.F., 1985. Carbonate platform facies models. American Association of Petroleum Geologists Bulletin 69, 1–21.
Reitner, J., 1993. Modern cryptic microbialite/metazoan faciesfrom Lizard Island (Great Barrier Reef, Australia), formationand concepts. Facies 29, 3–40.
Reolid, J., Betzler, C., Braga, J.C., Martin, J.M., Lindhorst, S., Reijmer, J.G., 2014. Reef slope geometries and facies distribution: controlling factors (Messinian, SE Spain). Facies 60, 737–753.
Reolid, J., Betzler, C., Eberli, G.P., Grammer, G.M., 2017. The importance of microbial binding in Neogene–Quaternary steep slopes. Journal of Sedimentary Research 87, 567–577. https://doi.org/10.2110/jsr.2017.28.
Romero, J., Caus, E., Rossel, J., 2002. A model for thepalaeoenvironmental distribution of larger foraminifera based on late Middle Eocene deposits on the margin of the south Pyrenean basin. Palaeogeography, Palaeoclimatology, Palaeoecology 179, 43–56.
Saltzman, M.R., Thomas, E., 2012. Carbon isotope stratigraphy. In: Gradstein, et al. (Eds.), The Geologic Time Scale. Elsevier, pp. 207–232 https://doi.org/10.1016/B978-0-444-59425-9.00011-1.
Schlager, W., 2005. Carbonate sedimentology and sequence stratigraphy. SEPM Concepts in Sedimentology and Paleontology 8, 200. https://doi.org/10.2110/csp.05.08.
Schrag, D.P., DePaolo, D.J., Richter, F.M., 1995. Reconstructing past sea surface temperatures: correcting for diagenesis of bulk marine carbonate. Geochimica et Cosmochimica Acta 59, 2265–2278. https://doi.org/10.1016/0016-7037(95)00105-9.
Serra-Kiel, J., Hottinger, L., Caus, E., Drobne, K., Ferrández, C., Jauhri, A.K., Less, G., Pavlovec, R., Pignatti, J.S., Samsó, J.M., Schaub, H., Sirel, E., Strougo, A., Tambareau, Y., Tosquella, J., Zakrevskaya, E., 1998. Larger Foraminiferal Biostratigraphy of the Tethyan Paleocene and Eocene. Bulletin de la Societé géologique de France 169, 281–299.
Spofforth, D.J.A., Agnini, C., Pälike, H., Rio, D., Fornaciari, E., Giusberti, L., Luciani, V., Lanci, L., Muttoni, G., 2010. Organic carbon burial following the middle Eocene climatic optimum in the central western Tethys. Paleoceanography 25, PA3210. https://doi.org/10.1029/2009PA001738.
Swart, P.K., 2015. The geochemistry of carbonate diagenesis: the past, present and future. Sedimentology 62, 1233–1304. https://doi.org/10.1111/sed.12205.
Tellini, A., 1890. Le nummuliti della Maiella, delle Isole Tremiti e del promontorio garganico. Bollettino della Societa Geologica Italiana 9, 359–422.
Tosquella, J., Martín-Martín, M., Guerrera, F., Serrano, F., Tramontana, M., 2022. The Eocene carbonate platform of the central-western Malaguides (Internal Betic Zone, S Spain) and its meaning for the Cenozoic paleogeography of the westermost Tethys. Palaeogeography, Palaeoclimatology, Palaeoecology 589, 110840. https://doi.org/10.1016/j.palaeo.2022.110840.
Ungaro, S., 1996. Adaptive morphological strategy of Gypsina (encrusting foraminifer). In: Cherchi, A. (Ed.), Autecology of Selected Fossil Organisms: Achievements and Problems. Bollettino della Società Paleontologica Italiana, Special Volume 3, pp. 233–241.
Van der Ploeg, R., Cramwinckel, M.J., Kocken, I.J., Leutert, T.J., Bohaty, S.M., Fokkema, C.D., Hull, P.M., Nele Meckler, A., Middelburg, J.J., Müller, I.A., Penman, D.E., Peterse, F., Reichart, G.J., Sexton, P.F., Vahlenkamp, M., De Vleeschouwer, D., Wilson, P.A., Ziegler, M., Sluijs, A., 2023. North Atlantic surface ocean warming and salinization in response to middle Eocene greenhouse warming. Science Advances 9, eabq0110. https://doi.org/10.1126/sciadv.abq0110.
Vecsei, A., Moussavian, E., 1997. Paleocene reefs in the Maiella platform margin, Italy: an example of the effects of the Cretaceous/Tertiary boundary events on reefs and carbonate platforms. Facies 36, 123–140.
Wendler, I., 2013. A critical evaluation of carbon isotope stratigraphy and biostratigraphic implications for Late Cretaceous global correlation. Earth-Science Reviews 126, 116–146. https://doi.org/10.1016/j.earscirev.2013.08.003.
Westerhold, T., Marwan, N., Drury, A.J., Liebrand, D., Agnini, C., Anagnostou, E., Barnet, J.S.K., Bohaty, S.M., De Vleeschouwer, D., Florindo, F., Frederichs, T., Hodell, D.A., Holbourn, A.E., Kroon, D., Lauretano, V., Littler, K., Lourens, L.J., Lyle, M., Pälike, H., Röhl, U., Tian, J., Wilkens, R.H., Wilson, P.A., Zachos, J.C., 2020. An astronomically dated record of Earth's climate and its predictability over the last 66 million years. Science 369, 1383–1387. https://doi.org/10.1126/science.aba6853.
Wilson, J.L., 1975. Carbonate Facies in Geologic History. Springer Verlag, New York, p. 471 https://doi.org/10.1007/978-1-4612-6383-8.
Wilson, M.E.J., 2008. Global and regional influences on equatorial shallow-marine carbonates during the Cenozoic. Palaeogeography, Palaeoclimatology, Palaeoecology 265, 262–274. https://doi.org/10.1016/j.palaeo.2008.05.012.
Zachos, J.C., Pagani, M., Sloan, L., Thomas, E., Billups, K., 2001. Trends, rhythms, and aberrations in global climate 65 Ma to present. Science 292, 686–693.
Zachos, J.C., McCarren, H., Murphy, B., Röhl, U., Westerhold, T., 2010. Tempo and scale of late Paleocene and early Eocene carbon isotope cycles: Implications for the origin of hyperthermals. Earth and Planetary Science Letters 299, 242–249. https://doi.org/10.1016/j.epsl.2010.09.004.